Acknowledgements We are grateful to the patient and his family for their participation. We also thank Takeda Pharmaceutical Company (Osaka, Japan) for kindly providing recombinant IL-2.

Authors' contributions T.K. performed experiments and wrote the paper. M.S. and Ka.I. performed experiments. R.N. designed the research, wrote the paper and analyzed data. Y.T. wrote the paper and analyzed data. T.M. treated the patient and analyzed data. S.O., Y.M., N.N., Ko.I, S.N., T.W. and A.Y. performed experiments and discussed the research. T.H. and T.N. designed the research.

Conflict of Interests The authors declare no competing financial interests.

References

1. Buckley RH. Primary immunodeficiency diseases: dissectors of the immune system. Immunol Rev. 2002;185:206–19.
2. Stephan V, Wahn V, Le Deist F, Dirksen U, Broker B, Muller-Fleckenstein I, et al. Atypical X-linked severe combined immunodeficiency due to possible spontaneous reversion of the genetic defect in T cells. N Engl J Med. 1996;335(21):1563–7.
3. Speckmann C, Pannicke U, Wiech E, Schwarz K, Fisch P, Friedrich W, et al. Clinical and immunologic consequences of a somatic reversion in a patient with X-linked severe combined immunodeficiency. Blood. 2008;112(10):4090–7.
4. Hirschhorn R, Yang DR, Puck JM, Huie ML, Jiang CK, Kurlandsky LE. Spontaneous in vivo reversion to normal of an inherited mutation in a patient with adenosine deaminase deficiency. Nat Genet. 1996;13(3):290–5.
5. Hirschhorn R. In vivo reversion to normal of inherited mutations in humans. J Med Genet. 2003;40(10):721–8.
6. Ariga T, Kondoh T, Yamaguchi K, Yamada M, Sasaki S, Nelson DL, et al. Spontaneous in vivo reversion of an inherited mutation in the Wiskott-Aldrich syndrome. J Immunol. 2001;166(8):5245–9.
7. Wada T, Toma T, Okamoto H, Kasahara Y, Koizumi S, Agematsu K, et al. Oligoclonal expansion of T lymphocytes with multiple second-site mutations leads to Omenn syndrome in a patient with RAG1-deficient severe combined immunodeficiency. Blood. 2005;106(6):2099–101.
8. Nishikomori R, Akutagawa H, Maruyama K, Nakata-Hizume M, Ohmori K, Mizuno K, et al. X-linked ectodermal dysplasia and immunodeficiency caused by reversion mosaicism of NEMO reveals a critical role for NEMO in human T-cell development and/or survival. Blood. 2004;103(12):4565–72.
9. Uzel G, Tng E, Rosenzweig SD, Hsu AP, Shaw JM, Horwitz ME, et al. Reversion mutations in patients with leukocyte adhesion deficiency type-1 (LAD-1). Blood. 2008;111(1):209–18.
10. Ariga T, Oda N, Yamaguchi K, Kawamura N, Kikuta H, Taniuchi S, et al. T-cell lines from 2 patients with adenosine deaminase (ADA) deficiency showed the restoration of ADA activity resulted from the reversion of an inherited mutation. Blood. 2001;97(9):2896–9.
11. Konno A, Okada K, Mizuno K, Nishida M, Nagaoki S, Toma T, et al. CD8alpha alpha memory effector T cells descend directly from clonally expanded CD8alpha+ beta high TCRalpha beta T cells in vivo. Blood. 2002;100(12):4090–7.
12. Sadaoka K, Okamoto S, Gomi Y, Tanimoto T, Ishikawa T, Yoshikawa T, et al. Measurement of varicella-zoster virus (VZV)-specific cell-mediated immunity: comparison between VZV skin test and interferon-gamma enzyme-linked immunospot assay. J Infect Dis. 2008;198(9):1327–33.
13. Kamiya H, Ihara T, Hattori A, Iwasa T, Sakurai M, Izawa T, et al. Diagnostic skin test reactions with varicella virus antigen and clinical application of the test. J Infect Dis. 1977;136(6):784–8.
14. Morinishi Y, Imai K, Nakagawa N, Sato H, Horiuchi K, Ohtsuka Y, et al. Identification of severe combined immunodeficiency by T-cell receptor excision circles quantification using neonatal guthrie cards. J Pediatr. 2009;155(6):829–33.
15. Tassara C, Pepper AE, Puck JM. Intronic point mutation in the IL2RG gene causing X-linked severe combined immunodeficiency. Hum Mol Genet. 1995;4(9):1693–5.
16. Reese MG, Eeckman FH, Kulp D, Haussler D. Improved splice site detection in Genie. J Comput Biol. 1997;4(3):311–23.
17. Sleasman JW, Harville TO, White GB, George JF, Barrett DJ, Goodenow MM. Arrested rearrangement of TCR V beta genes in thymocytes from children with X-linked severe combined immunodeficiency disease. J Immunol. 1994;153(1):442–8.
18. Joachims ML, Chain JL, Hooker SW, Knott-Craig CJ, Thompson LF. Human alpha beta and gamma delta thymocyte development: TCR gene rearrangements, intracellular TCR beta expression, and gamma delta developmental potential–differences between men and mice. J Immunol. 2006;176(3):1543–52.
19. Freitas AA, Rocha B. Population biology of lymphocytes: the flight for survival. Annu Rev Immunol. 2000;18:83–111.
20. Appay V, van Lier RA, Sallusto F, Roederer M. Phenotype and function of human T lymphocyte subsets: consensus and issues. Cytometry A. 2008;73(11):975–83.

Int J Hematol (2012) 95:692–696
DOI 10.1007/s12185-012-1055-4

CASE REPORT

Delayed onset adenosine deaminase deficiency associated with acute disseminated encephalomyelitis

Hideyuki Nakaoka · Hirokazu Kanegane · Hiromichi Taneichi · Kazushi Miya · Xi Yang · Keiko Nomura · Shunichiro Takezaki · Masafumi Yamada · Osamu Ohara · Chikako Kamae · Kohsuke Imai · Shigeaki Nonoyama · Taizo Wada · Akihiro Yachie · Michael S. Hershfield · Tadashi Ariga · Toshio Miyawaki

Received: 23 June 2011 / Revised: 8 March 2012 / Accepted: 9 March 2012 / Published online: 24 March 2012

Abstract Acute disseminated encephalomyelitis (ADEM) is a monophasic, immune-mediated demyelinating disorder that can appear after either immunizations or, more often, infections. Magnetic resonance imaging of patients shows inflammatory lesions in the brain and spinal cord. An immune-mediated mechanism may play a role in this disease, although its precise pathogenesis remains unclear. In this study, a 2-year-old boy presented with ADEM, and he showed improvement on treatment with high-dose intravenous corticosteroids. At the age of 3 years, the presence of recurrent bronchitis, bronchiectasia, and lymphopenia suggested that the patient was suffering from combined immunodeficiency. The patient was finally diagnosed with delayed onset adenosine deaminase deficiency. Delayed onset adenosine deaminase deficiency is frequently associated with autoimmune diseases, including thyroiditis and cytopenia, both of which were observed in the patient. The ADEM in this patient may be a presentation of delayed onset adenosine deaminase deficiency.

Keywords Acute disseminated encephalomyelitis · Adenosine deaminase · Bronchiectasia · Delayed onset · Lymphopenia

H. Nakaoka · H. Kanegane (✉) · H. Taneichi · K. Miya · X. Yang · K. Nomura · T. Miyawaki
Department of Pediatrics, Graduate School of Medicine and Pharmaceutical Sciences, University of Toyama, 2630 Sugitani, Toyama, Toyama 930-0194, Japan
e-mail: kanegane@med.u-toyama.ac.jp

S. Takezaki · M. Yamada · T. Ariga
Department of Pediatrics, Hokkaido University Graduate School of Medicine, Sapporo, Japan

O. Ohara
Department of Human Genome Research, Kazusa DNA Research Institute, Kisarazu, Japan

C. Kamae · K. Imai · S. Nonoyama
Department of Pediatrics, National Defense Medical College, Tokorozawa, Japan

T. Wada · A. Yachie
Department of Pediatrics, School of Medicine, Institute of Medical, Pharmaceutical and Health Sciences, Kanazawa University, Kanazawa, Japan

M. S. Hershfield
Duke University Medical Center, Durham, NC, USA

Introduction

Adenosine deaminase (ADA) deficiency is a systemic purine metabolic disorder that primarily affects lymphocyte development and function [1, 2]. ADA deficiency has accounted for approximately 15 % of severe combined immunodeficiency (SCID) cases and 30–40 % of autosomal recessive SCID cases [3]. The *ADA* gene is encoded by a 32 kb region that contains 12 exons and is located in chromosome 20q13.11, and *ADA* mutations include missense, splicing, deletion and nonsense mutations. ADA is an enzyme of the purine salvage pathway that catalyzes the deamination of adenosine and deoxyadenosine, giving rise to inosine and deoxyinosine, respectively. The absence of ADA results in an accumulation of the substrate adenosine and deoxyadenosine. The latter is phosphorylated by nucleoside kinases, which results in the production of deoxynucleotide triphosphates (dATP). ADA deficiency may promote pro-apoptotic effects due to the accumulation of dATP, which may be responsible for the observed lymphopenia due to ADA deficiency. Thus, the clinical presentation of ADA-deficient patients is similar to that of SCID patients.

A majority of ADA-deficient patients have neonatal-onset disease and present with lymphopenia, an absence of cellular and humoral immunity, failure to thrive and a rapid disease course due to infections. However, approximately 15 % of ADA-deficient patients are diagnosed between 3 and 15 years of age or in adulthood, and their disorder has been referred to as "delayed onset type" and "late onset type" ADA deficiency. Patients with delayed onset ADA deficiency show variable clinical manifestations including recurrent sinopulmonary bacterial infections and septicemia. Laboratory data may show IgG2 deficiency, but a markedly elevated IgE titer and eosinophilia. Autoimmune diseases, including autoimmune hypothyroiditis, diabetes mellitus, hemolytic anemia and idiopathic thrombocytopenia, may be observed in conjunction with ADA deficiency. Here, we describe a Japanese child with delayed onset ADA deficiency.

Before the time of diagnosis, the patient had acute disseminated encephalomyelitis (ADEM), from which he recovered with minor residual disability. ADEM shows multiple inflammatory lesions in the brain and spinal cord, particularly in the white matter, suggesting that it may involve autoimmune demyelination [4]. Therefore, ADEM may be an early sign of autoimmune disease resulting from the onset of delayed onset ADA deficiency as autoimmune disease.

Case report

The patient had experienced recurrent bronchitis and mild leukopenia since 5 months of age, but the patient had no severe infections or adverse effects. At 2 years of age, he presented with a fever, gait disturbances and lethargy, and he was admitted to the hospital. Upon admission, he also had motor weakness and urinary retention. Physical examination revealed drowsiness and bilateral normal deep tendon reflexes, but no neck stiffness was observed. Laboratory investigations, which included a measure of antinuclear antibody titers, were normal. Cerebrospinal fluid (CSF) analysis revealed 51 white blood cells per microliter with 86 % lymphocytes and 14 % polymorphonuclear cells, and the total protein content was increased to 102 mg/dl. CSF culture was negative and the glucose level was normal. Myelin basic protein in CSF was increased to 5347 pg/ml (normal <102 pg/ml), suggesting the occurrence of demyelination. Magnetic resonance imaging (MRI) showed patch lesions of high signal intensity on the T2-weighted images and low signal on the T1-weighted images in the subcortical and central white matter regions, as well as the basal ganglia and spine (Fig. 1). These findings suggested demyelination and edema. Multiple asymmetric lesions were present.

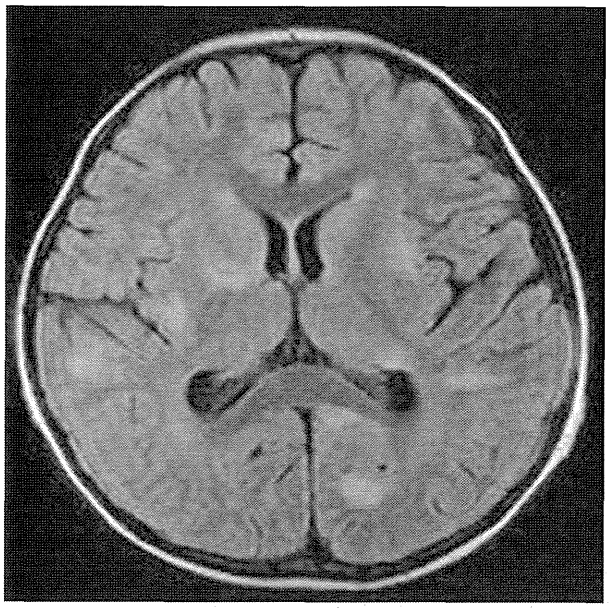

Fig. 1 Axial T2-weighted MRI of the patient's brain. Several high intensity signals are observed in the brain, as indicated

The clinical and MRI data led us to the diagnosis of ADEM, and the patient was immediately treated with high-dose intravenous methylprednisolone. The patient's level of consciousness and his neurological signs gradually improved over the next month. He retained only a residual hyperreflexia of the patella and Achilles tendons. Four months later, the brain MRI results were almost normal.

Frequent infectious episodes were again observed in the patient after he turned 3 years old, and he was finally admitted for investigation. A physical examination revealed that the boy's height was 100 cm (+0.5 SD), and his weight was 16.2 kg (+0.7 SD). Other clinical statistics were as follows: his temperature was 37.4 °C, heart rate was 135/min, respiratory rate was 25/min, blood pressure was 102/62 mmHg and SpO_2 was 95 % at room temperature. Occasional rales were heard over both lungs. Neither organomegaly nor enlarged lymph nodes were observed.

Laboratory tests revealed altered contributions of blood cells, but largely normal blood chemistry. The specific blood values recoded are as follows: hemoglobin, 10.2 g/dl; white blood cells, 2220/μl with 600/μl neutrophils and 580/μl lymphocytes; platelets, 276000/μl; and C-reactive protein, 4.43 mg/dl (normal range <0.29 mg/dl). Blood chemistry, which included liver enzymes and electrolytes, was normal. Chest X-rays appeared normal, although chest computed tomography revealed bronchiectasia. KL-6 was elevated to 3674 U/ml (normal <499 U/ml). Thyroid-stimulating hormone was elevated to 133 μIU/ml (normal 0.35–3.73 μIU/ml). However, free T3 and free T4 were roughly normal at 2.3 pg/ml (normal 2.2–4.1 pg/ml) and

0.6 ng/dl (normal 0.9–1.8 ng/dl), respectively. These data suggest that the patient had hypothyroidism. The presence of anti-thyroglobulin and anti-thyroid peroxidase antibodies indicated autoimmune thyroiditis, and the patient was treated with levothyroxine.

Unexpectedly, immunological studies showed hypergammaglobulinemia in the patient (Table 1). IgG2 levels were within the normal range, but a percentage of an IgG2 subclass (5.41 %) was lower than that in the normal controls (20–30 %). In addition, the patient tested positive for varicella zoster-specific IgG. Although the patient had recurrent pneumococcal infections, the level of pneumococcus-specific IgG2 was only 0.6 μg/ml (normal >3.0 μg/ml). Lymphocyte subpopulations revealed an extremely high frequency of activated (HLA-DR$^+$) CD3$^+$ T cells and memory (CD45RO$^+$) CD4$^+$ and CD8$^+$ T cells, and an extremely reduced number of CD20$^+$ B cells. An analysis of the T-cell receptor Vβ repertoire revealed a strongly skewed pattern in CD8$^+$ T cells but not in the repertoire of CD4$^+$ T cells (data not shown). Lymphocyte proliferation was impaired in response to phytohemagglutinin, and natural killer cell activity was low. T-cell receptor excision circles (TRECs) were quantified by real time-PCR, as previously described [5]. When measured with the patient's neonatal Guthrie card, the copy number of TRECs was lower than normal, but they were well detectable. However, TRECs were undetectable in this patient at the age of 3 years. The delayed-type hypersensitivity skin test, which uses purified protein from tuberculosis, was negative despite the fact that the patient had been immunized with the bacille Calmette–Guérin vaccine. Furthermore, the patient was positive for various autoantibodies, including anti-thyroglobulin and anti-nuclear antibodies.

Table 1 Immunological studies in the patient

Test	Value	Unit	Normal value
Immunoglobulins			
IgG	1659	mg/dl	929 ± 228
IgA	51	mg/dl	56 ± 18
IgM	188	mg/dl	93 ± 27
IgE	62	IU/ml	0–170
IgG subclasses			
IgG1	1220	mg/dl	390.2–955.2
IgG2	72.9	mg/dl	58.5–292.1
IgG3	52.4	mg/dl	11.4–98.8
IgG4	3.0	mg/dl	1.2–76.7
Lymphocyte subpopulations			
CD3	70.3	%	71.4 ± 5.8
CD4	23.4	%	43.2 ± 11.5
CD8	44.2	%	22.3 ± 6.6
HLA-DR/CD3	76.5	%	<1.0
CD45RO/CD4	74.8	%	21.9 ± 4.4
CD45RO/CD8	39.6	%	14.9 ± 5.6
CD20	0.2	%	12.5 ± 6.7
Lymphoproliferative response to mitogen			
Phytohemagglutinin	7438	cpm	20500–56800
Natural killer cell activity	6	%	18–40
TRECs quantification			
At birth	1.011×10^3	copies/μg DNA	$6.2 \pm 3.2 \times 10^3$
Present	Undetectable		
Autoantibodies			
Anti-thyroglobulin	538	IU/ml	<27.9
Anti-thyroid peroxidase	185	U/ml	<0.29
Anti-nuclear	Positive		Negative
Anti-neutrophil	Positive		Negative

Although the patient showed hypergammaglobulinemia, the presence of humoral and cellular immune defects in addition to various autoimmune features suggested a diagnosis of delayed onset ADA deficiency. Therefore, ADA enzyme activity was assayed by the radiochemical thin-layer chromatography method, as previously described [6, 7]. The levels of adenosine nucleotide (AXP) and deoxyadenosine nucleotides (dAXP) in erythrocytes were determined, as previously described [8]. The patient's ADA activity in mononuclear cells was detectable at 8.6 nmol/min/10^8 cells, but this value is approximately one-tenth of activity found in normal controls (102.6 nmol/min/10^8 cells) (Fig. 2). Consistent with this observation, the patient's ADA level in red blood cells (RBC) was 0 nmol/h/mg (normal 26.4 ± 10.0 nmol/h/mg), and the toxic metabolite dAXP levels in RBC were increased to 9.4 % (normal <1 %). These data indicated that the ADA activity observed in the patient might be mild. The parents' ADA levels in RBC were intermediate between that of the patient's level and that of a normal control (mother

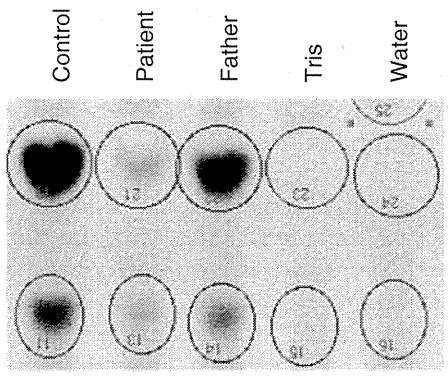

Fig. 2 ADA enzymatic activity. Each lane corresponds to a different sample as follow: control individual (102.6 U), the patient (8.6 U), the patient's father (39.6 U), Tris (1.0 U), and water (1.0 U). U denotes nmol/min/10^8 cells

12.2 nmol/h/mg, father 14.1 nmol/h/mg), which suggests that they are carriers of the ADA deficiency. Gene analysis of *ADA* revealed compound heterozygous mutations in the patient (R156C and V177M), each contributed by one parent: the mother had contributed the R156C mutation and the father passed on a V177M mutation, respectively, thereby confirming the parents' carrier status.

After the diagnosis of delayed onset ADA deficiency, the patient was treated with intravenous immunoglobulin, and he received oral administration of trimethoprim–sulfamethoxazole, and acyclovir. Following the prophylactic treatment, the patient was nearly free from infections. However, serum immunoglobulin levels were decreased (IgG 1069 mg/dl, IgA 21 mg/dl, and IgM 33 mg/dl) at the age of 4 years. Therefore, we searched for a human leukocyte antigen-identical donor and identified his healthy sister as a suitable donor. At the age of 4 years, he underwent a bone marrow transplant preceded by a reduced-intensity conditioning regimen. This regimen included reduced dose intravenous busulfan (8.8 mg/kg total) and fludarabine (total dose: 180 mg/m^2) with standard cyclosporine A prophylaxis. Total nucleated cell and CD34$^+$ cell counts were 6.9×10^8 and 3.1×10^6 cells/kg, respectively. Thus, the patient's condition was good and he exhibited immune reconstitution with nearly complete chimerism.

Discussion

The recurrent infectious episodes in the patient presented herein suggested that he harbored a primary immunodeficiency, and bronchiectasis demonstrated by computed tomography strongly suggested that it was specially a humoral immunodeficiency. Although he had hypergammaglobulinemia, the relatively low frequency of IgG2 subclasses, low levels of pneumococcus-specific IgG2 and the decreased number of B cells demonstrated that the patient had humoral immune defects. Nonetheless, the absolute number of T cells was decreased, and naïve T cells were profoundly diminished in the patient. Impaired lymphocyte proliferation in response to mitogen and the lack of TRECs also indicated that a cellular immune deficiency was present. Hyperproduction of immunoglobulins by scanty B cells suggests that the patient's B cells may be oligoclonal. Furthermore, it remains to be determined whether a specific autoantibody target could be associated with the development of ADEM in this patient, particularly because he also presented with autoimmune disease, such as autoimmune thyroiditis. The combined presence of delayed onset combined immune deficiency and autoimmunity suggested a diagnosis of either delayed onset ADA deficiency or RAG deficiency. Our patient was finally diagnosed with delayed onset ADA deficiency.

The various phenotypes observed in ADA deficiency exhibit a strong correlation with their respective genotypes. For instance, alleles are grouped according to the resulting levels of ADA activity: deletion and nonsense alleles formed Group 0, which assumes no activity, whereas the amino acid substitutions are placed in Groups I–IV with increasing ADA activity [9]. The levels of soluble ADA activity and immunoreactive ADA protein expressed by mutant *ADA* cDNA were measured. ADA proteins bearing the patient's R156C or V177M mutations were included in Groups I and II, respectively. Patients with Group 0 or I alleles might show SCID, whereas patients with Group II might present with delayed onset phenotypes. The phenotype resulting from a combination of R156C and V177M mutations is compatible with that of delayed onset ADA deficiency.

ADEM is defined as a first episode of inflammatory demyelination with polyfocal neurological deficits (altered behavior or consciousness) [4]. MRI features of diffuse, bilateral lesions support ADEM. While the pathophysiology of ADEM remains undefined, it is believed to include autoimmune responses mounted de novo or following an infection. There is no report of an association between ADEM and ADA deficiency, although ADEM is rarely associated with immune deficient individuals. For instance, in one report, a child with common variable immune deficiency was associated with ADEM and Lennox–Gastaut syndrome [10], and ADEM has been observed in several patients with primary HIV infections [11–14]. Abnormal T cells and/or B cells that may be present under conditions of immune deficiency may promote an autoimmune process that results in ADEM. In support of this notion, patients with delayed onset ADA deficiency are frequently associated with autoimmune diseases, including autoimmune thyroiditis. The combination of an oligoclonal T-cell repertoire and a specific autoantibody produced by B cells may contribute to the development of ADEM in the patient. This study suggested that the patient presented ADEM as an autoimmune disease associated with delayed onset ADA deficiency.

Acknowledgments We thank Mr. Hitoshi Moriuchi and Ms. Chikako Sakai for their excellent technical assistance. This work was supported by a Grant-in-Aid for Scientific Research from the Ministry of Education, Culture, Sports, Science and Technology of Japan; and a grant for Research on intractable diseases from the Ministry of Health, Labour, and Welfare of Japan, Tokyo.

References

1. Hershfiled MS. Combined immune deficiency due to purine enzyme defects. In: Stiehm ER, Ochs HD, Winkelstein JA, editors. Immunologic disorders in infants and children. Philadelphia: WB Saunders; 2004. p. 480–504.

2. Hirschhorn R, Candotti F. Immunodeficiency disease due to defects of purine metabolism. In: Ocs HD, Smith CIE, Puck JM, editors. Primary immunodeficiency diseases: a molecular and genetic approach. New York: Oxford University Press; 2007. p. 169–96.
3. Buckley RH, Schiff RI, Schiff SE, et al. Human severe combined immunodeficiency: genetic, phenotypic, and functional diversity in one hundred eight infants. J Pediatr. 1997;130:378–87.
4. Dale RC, Brilot F, Banwell B. Pediatric central nervous system inflammatory demyelination: acute disseminated encephalomyelitis, clinically isolated syndrome, neuromyelitis optica, and multiple sclerosis. Curr Opin Neurol. 2009;22:233–40.
5. Morinishi Y, Imai K, Nakagawa N, et al. Identification of severe combined immunodeficiency by T-cell receptor excision circles quantification using neonatal Guthrie cards. J Pediatr. 2009;155:829–33.
6. Ariga T, Oda N, Yamaguchi K, et al. T-cell lines from 2 patients with adenosine deaminase (ADA) deficiency showed restoration of ADA activity resulted from the reversion of an inherited mutation. Blood. 2001;97:2896–9.
7. Kohn DB, Mitsuya H, Ballow M, et al. Establishment and characterization of adenosine deaminase-deficient human T cell lines. J Immunol. 1989;142:3971–7.
8. Hershfield MS, Buckley RH, Greenberg ML, et al. Treatment of adenosine deaminase deficiency with polyethylene glycol-modified adenosine deaminase. N Engl J Med. 1987;316:589–96.
9. Arredondo-Vega FX, Santisteban I, Daniels S, Toutain S, Hershfield MS. Adenosine deaminase deficiency: genotype-phenotype correlations based expressed activity of 29 mutant alleles. Am J Hum Genet. 1998;63:1049–59.
10. Kondo M, Fukao T, Teramoto T, et al. A common variable immunodeficient patient who developed acute disseminated encephalomyelitis followed by the Lennox-Gastaut syndrome. Pediatr Allergy Immunol. 2005;16:357–60.
11. Allen SH, Malik O, Lipman MCI, Johnson MA, Wilson LA. Acute demyelinating encephalitis (ADEM) in a patient with HIV infection. J Infect. 2002;45:62–4.
12. Morgensen TH, Marinovskij E, Larsen CS. Acute demyelinizating encephalomyelitis (ADEM) as initial presentation of primary HIV infection. Scand J Infect Dis. 2007;39:630–4.
13. Narciso P, Galgani S, Del Grosso B, et al. Acute disseminated encephalomyelitis as manifestation of primary HIV infection. Neurology. 2001;57:1493–6.
14. van Toorn R, Kritzinger F, Rabie H. Acute demyelinating encephalomyelitis (ADEM), cryptococcal reactivation and disseminated Herpes simplex in an HIV infected child following HAART. Eur J Pediatr Neurol. 2005;9:355–9.

Wnt3a stimulates maturation of impaired neutrophils developed from severe congenital neutropenia patient-derived pluripotent stem cells

Takafumi Hiramoto[a,b], Yasuhiro Ebihara[b,c,1], Yoko Mizoguchi[d], Kazuhiro Nakamura[d], Kiyoshi Yamaguchi[e], Kazuko Ueno[f], Naoki Nariai[f], Shinji Mochizuki[b,c], Shohei Yamamoto[b,c], Masao Nagasaki[f], Yoichi Furukawa[e], Kenzaburo Tani[a], Hiromitsu Nakauchi[g], Masao Kobayashi[d], and Kohichiro Tsuji[b,c]

[a]Division of Molecular and Clinical Genomics, Medical Institute of Bioregulation, Kyushu University, Higashi-ku, Fukuoka 812-8582, Japan; [c]Department of Pediatric Hematology/Oncology, Research Hospital, Divisions of [b]Stem Cell Processing and [g]Stem Cell Therapy, Center for Stem Cell Biology and Regenerative Medicine, and [e]Division of Clinical Genome Research, Advanced Clinical Research Center, Institute of Medical Science, University of Tokyo, Minato-ku, Tokyo 108-8639, Japan; [d]Pediatrics, Hiroshima University Graduate School of Biomedical and Health Sciences, Minami-ku, Hiroshima 734-8551, Japan; and [f]Department of Integrative Genomics, Tohoku Medical Megabank Organization, Tohoku University, Aramaki, Aoba-ku, Sendai 980-8573, Japan

Edited by George Q. Daley, Children's Hospital Boston, Boston, MA, and accepted by the Editorial Board January 4, 2013 (received for review October 1, 2012)

The derivation of induced pluripotent stem (iPS) cells from individuals of genetic disorders offers new opportunities for basic research into these diseases and the development of therapeutic compounds. Severe congenital neutropenia (SCN) is a serious disorder characterized by severe neutropenia at birth. SCN is associated with heterozygous mutations in the neutrophil elastase [elastase, neutrophil-expressed (ELANE)] gene, but the mechanisms that disrupt neutrophil development have not yet been clarified because of the current lack of an appropriate disease model. Here, we generated iPS cells from an individual with SCN (SCN-iPS cells). Granulopoiesis from SCN-iPS cells revealed neutrophil maturation arrest and little sensitivity to granulocyte-colony stimulating factor, reflecting a disease status of SCN. Molecular analysis of the granulopoiesis from the SCN-iPS cells vs. control iPS cells showed reduced expression of genes related to the wingless-type mmtv integration site family, member 3a (Wnt3a)/β-catenin pathway [e.g., lymphoid enhancer-binding factor 1], whereas Wnt3a administration induced elevation lymphoid enhancer-binding factor 1-expression and the maturation of SCN-iPS cell-derived neutrophils. These results indicate that SCN-iPS cells provide a useful disease model for SCN, and the activation of the Wnt3a/β-catenin pathway may offer a novel therapy for SCN with ELANE mutation.

apoptosis | unfolded protein response | SCN disease model

Severe congenital neutropenia (SCN) is a heterogeneous bone marrow (BM) failure syndrome characterized by severe neutropenia at birth, leading to recurrent infections by bacteria or fungi (1). SCN patients reveal an arrest in neutrophil differentiation in the BM at the promyelocyte or myelocyte stage (1), as well as a propensity to develop myelodysplastic syndrome and acute myeloid leukemia (2). Current treatment by high-dose granulocyte-colony stimulating factor (G-CSF) administration induces an increase in the number of mature neutrophils in the peripheral blood of most SCN patients (3). Although this treatment is curative for the severe infections, there is a concern that high-dose G-CSF may increase the risk of hematologic malignancy in these individuals (4).

Several genetic mutations have been identified in SCN patients. Approximately 50% of autosomal-dominant SCN cases were shown to have various heterozygous mutations in the gene encoding neutrophil elastase [elastase, neutrophil-expressed (ELANE)] (5, 6), a monomeric, 218-amino acid (25 kDa) chymotryptic serine protease (7) that is synthesized during the early stages of primary granule production in promyelocytes (8, 9). However, the mechanism(s) causing impaired neutrophil maturation in SCN patients remains unclear due to the current lack of an appropriate disease model.

Results and Discussion

In the present study, we generated induced pluripotent stem (iPS) cells from the BM cells obtained from an SCN patient with a heterologous ELANE gene mutation (exon 5, 707 region, C194X) (SCN-iPS cells) to provide the basis for an SCN disease model. The patient who donated BM cells recurrently suffered from severe infections without exogenous G-CSF administration, but the G-CSF administration once a week prevented his repeated infection. The SCN-iPS cells continued to show embryonic stem cell morphology after >20 passages and also expressed pluripotent markers (Fig. S1*A*). The silencing of exogenous genes and the capability to differentiate into three germ layers by teratoma formation were confirmed for each of the three SCN-iPS cell clones (Fig. S1 *B* and *C*). Furthermore, the same ELANE gene mutation that was present in the patient persisted in the SCN-iPS cells (Fig. S1*D*). The SCN-iPS cells, as well as control iPS cells that were generated from healthy donors, had the normal karyotype (Fig. S1*E*) (10, 11) and no mutations in the mutation-sensitive region of the G-CSF receptor gene (12).

We first compared the hematopoietic differentiation from SCN-iPS cells with that from control iPS cells that were generated from healthy donors. SCN-iPS and control iPS cells were cocultured with a 15-Gy-irradiated murine stromal cell line (the AGM-S3 cell line), as reported (13). After 12 d, the cocultured cells were harvested, and the $CD34^+$ cells separated from these cells (SCN-iPS–$CD34^+$ and control iPS–$CD34^+$ cells, respectively) were cultured in a hematopoietic colony assay by using a cytokine mixture (*Materials and Methods*). The number and size of the erythroid (E) and mixed-lineage (Mix) colonies derived from SCN-iPS–$CD34^+$ cells (1×10^4 cells) were nearly identical to those of the corresponding colonies derived from control iPS–$CD34^+$ cells (E colonies: SCN-iPS cells, 11.0 ± 3.0, and control iPS cells, 11.4 ± 3.9; Mix colonies: SCN-iPS cells, 25.1 ± 7.2, and control iPS cells, 17.4 ± 4.0) (Fig. 1 *B* and *C* and Fig. S2 *A* and *B*). However, the number of myeloid colonies derived from SCN-iPS–$CD34^+$ vs. control iPS–$CD34^+$ cells was significantly lower (SCN-iPS cells, 47.4 ± 19.5; control iPS cells, 127.8 ± 17.9; $P < 0.01$), and the size of the colonies was also smaller (Fig. 1 *A*

Author contributions: T.H., Y.E., K.Y., S.M., S.Y., Y.F., K. Tani, H.N., M.K., and K. Tsuji designed research; T.H., Y.M., K.N., and K.Y. performed research; T.H., Y.E., Y.M., K.N., K.Y., K.U., N.N., S.M., S.Y., M.N., and K. Tsuji analyzed data; and T.H., Y.E., and K. Tsuji wrote the paper.

The authors declare no conflict of interest.

This article is a PNAS Direct Submission. G.Q.D. is a guest editor invited by the Editorial Board.

[1]To whom correspondence should be addressed. E-mail: ebihara@ims.u-tokyo.ac.jp.

This article contains supporting information online at www.pnas.org/lookup/suppl/doi:10.1073/pnas.1217039110/-/DCSupplemental.

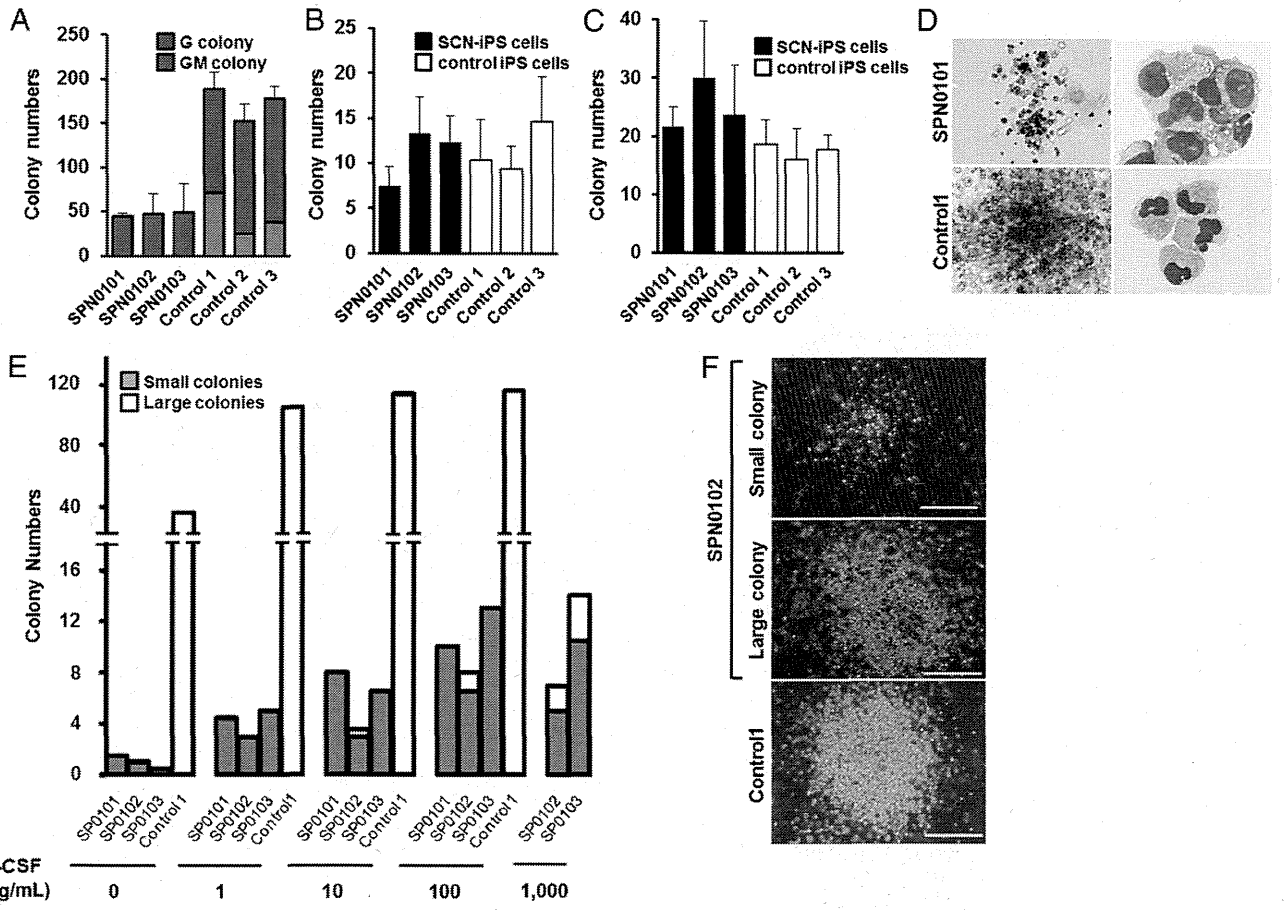

Fig. 1. Impaired neutrophil development from SCN-iPS cells. (*A*–*C*) A hematopoietic colony assay was performed by using 1×10^4 $CD34^+$ cells derived from three SCN-iPS cell clones (SPN0101, SPN0102, and SPN0103) and three control iPS cell clones (controls 1, 2, and 3) in the presence of a cytokine mixture. Colonies were sorted as myeloid (*A*), erythroid (*B*), and mixed-lineage (Mix) (*C*). Data are shown as mean ± SD. (*D*) Photographs of colonies (*Left*; 100×) and cells in a GM colony (*Right*; 400×; May–Grünwald–Giemsa staining). (*E*) A hematopoietic colony assay with dose escalation of G-CSF was performed by using 1×10^5 $CD34^+$ cells derived from SCN-iPS and control iPS cells. Filled and open bars indicate small colonies consisting of <100 cells and large colonies consisting of >100 cells, respectively. Data are shown as the average of three independent experiments. (*F*) Photographs of a small colony derived from SCN-iPS cells (SPN0102) in the presence of 10 ng/mL G-CSF, large colonies derived from SCN-iPS cells in the presence of 1,000 ng/mL G-CSF, and large colonies derived from control iPS cells (control 1) in the presence of 10 ng/mL G-CSF. (Scale bars, 200 μm.)

and *D*). In particular, only a few SCN-iPS cell-derived granulocyte (G) colonies—myeloid colonies consisting of only granulocytes—were detected (Fig. 1*A*). SCN-iPS cell-derived granulocyte–macrophage (GM) colonies—myeloid colonies consisting of macrophages/monocytes with/without granulocytes—contained a few immature myeloid cells in addition to macrophages/monocytes, whereas control iPS cell-derived GM colonies included a substantial number of mature, segmented, and band neutrophils (Fig. 1*D*).

We also found that Mix colonies derived from SCN-iPS cells, but not control iPS cells, contained immature myeloid cells and few mature neutrophils (Fig. S2 *C* and *D*). Next, we conducted a hematopoietic colony assay using various concentrations of G-CSF alone instead of the cytokine mixture to examine the G-CSF dose dependency of neutrophil differentiation from SCN-iPS and control iPS–$CD34^+$ cells. For all concentrations of G-CSF used (1–1,000 ng/mL), the SCN-iPS cell-derived myeloid colonies were significantly lower in number and smaller in size than the control iPS cell-derived myeloid colonies (Fig. 1*E*). Myeloid colony formation from control iPS cells reached a plateau at ~1–10 ng/mL G-CSF, whereas the number and size of those from SCN-iPS cells gradually increased with increasing concentrations of G-CSF. However, the values observed for SCN-iPS cells did not reach those for the control iPS cells, even at the highest dose of G-CSF used (1,000 ng/mL). Furthermore, large colonies consisting of >100 cells derived from SCN-iPS cells were only found with higher concentrations of G-CSF (Fig. 1*F*). Thus, granulopoiesis initiated from SCN-iPS cells was relatively insensitive to G-CSF, reflecting the inadequate in vivo response of neutrophils to G-CSF in SCN patients (14, 15). Therefore, these results support the applicability of the SCN-iPS cells established herein as a disease model for SCN.

To examine neutrophil development from SCN-iPS cells in more detail, SCN-iPS and control iPS–$CD34^+$ cells (1×10^4 cells each) were cocultured in suspension with AGM-S3 cells in the presence of neutrophil differentiation medium (*SI Materials and Methods*). The number of nonadherent cells derived from SCN-iPS–$CD34^+$ cells was lower than that from control iPS–$CD34^+$ cells on day 14 of culture (SCN-iPS cells, $9.77 \times 10^4 \pm 1.65 \times 10^4$ cells; control iPS cells, $52.48 \times 10^4 \pm 23.13 \times 10^4$ cells; $P < 0.05$) (Fig. 2*A*). The proportion of mature neutrophils among the nonadherent cells was also significantly lower for SCN-iPS cells relative to control iPS cells on day 14 (SPN-iPS cells, 15.53% ± 4.33%; control iPS cells, 71.285 ± 3.30%; $P < 0.05$) (Fig. 2 *B* and *C*), indicating that myeloid cells derived from SCN-iPS cells revealed the maturation arrest in the neutrophil development. We then examined a possibility that the maturation arrest in SCN-

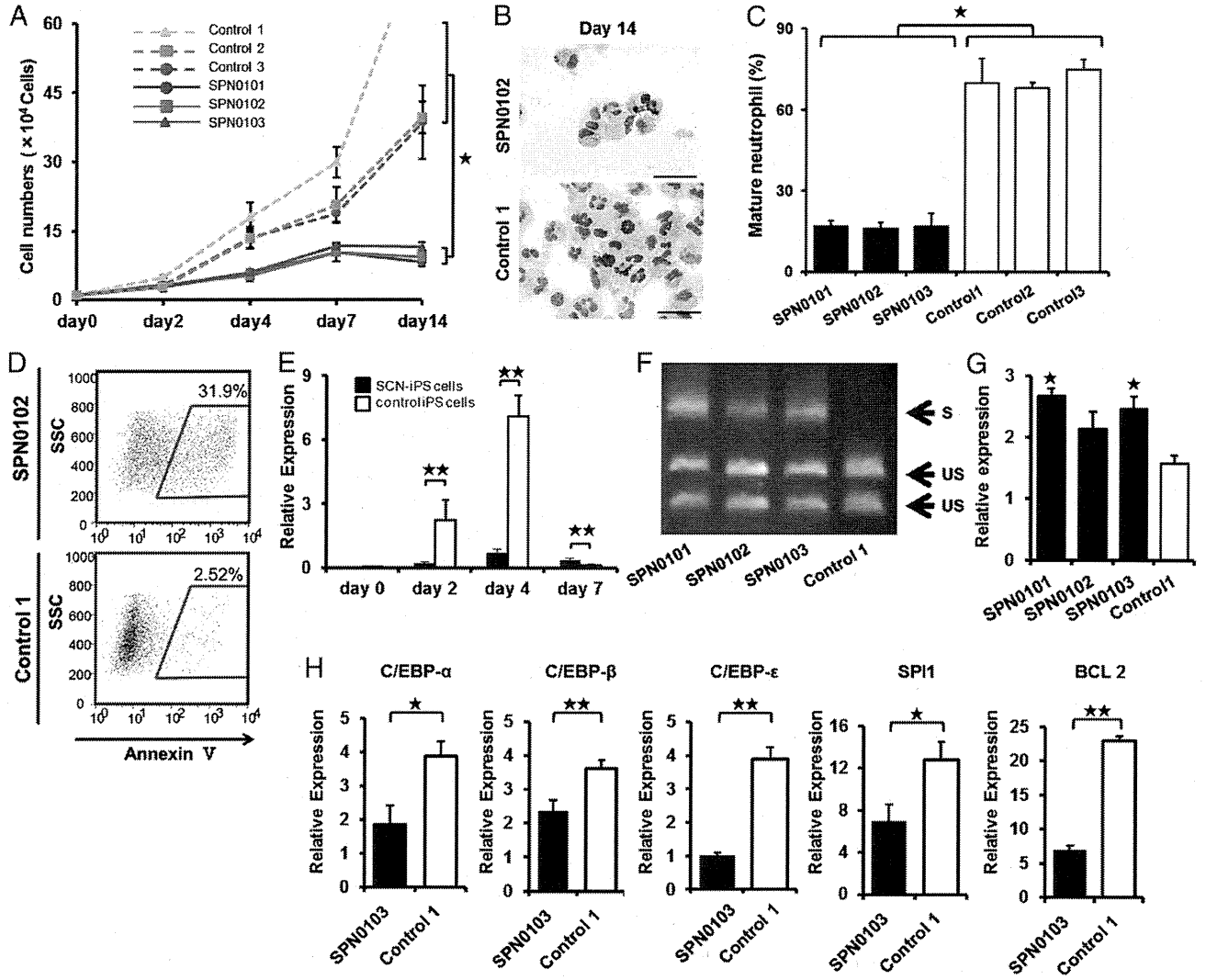

Fig. 2. Analysis of impaired neutrophil development from SCN-iPS cells. (*A*) Total number of nonadherent cells in the suspension culture of 1×10^4 $CD34^+$ cells derived from SCN-iPS and control iPS cells. Data are shown as mean ± SD. $^*P < 0.01$. (*B*) Photographs of nonadherent cells derived from SCN-iPS (SPN0103) and control iPS cells (control 1) on day 14 of culture (400×; May–Grünwald–Giemsa staining; scale bars, 50 μm.) (*C*) Filled and open bars show the proportion of mature neutrophils among the cells derived from SCN-iPS (filled bars) and control iPS (open bars) cells on day 14 of suspension culture. Data are shown as mean ± SD. $^*P < 0.05$. (*D*) Flow cytometric analysis of annexin V expression on cultured cells from SCN-iPS cells (SPN0102) or control iPS cells (control 1) on day 7. (*E*) Sequential qRT-PCR analysis of the relative expression of ELANE mRNA [ELANE/hypoxanthine–guanine phosphoribosyltransferase (HPRT) expression]. Data obtained from independent experiments using three SCN-iPS cell clones (SPN0101, SPN0102, and SPN0103) and three control iPS cell clones are shown as mean ± SD. $^{**}P < 0.01$. (*F* and *G*) $CD34^+$ cells derived from SCN-iPS or control iPS cells were cultured in neutrophil differentiation medium (see text). On day 7, nonadherent cells were collected and analyzed. (*F*) Representative gel showing spliced (S) and unspliced (US) XBP-1 bands on day 7. (*G*) qRT-PCR analysis of the relative mRNA expression (target/HPRT expression) of BiP on day 7. Data are shown as mean ± SD. $^*P < 0.05$; different from control 1). (*H*) qRT-PCR analysis of the relative mRNA expression (target / HPRT expression) of C/EBP-α, C/EBP-β, C/EBP-ε, SPI1, and BCL2 genes in non-adherent cells derived from SCN-iPS cells (filled bars, SPN0103) and control iPS cells (open bars, control 1) on day 2 of suspension culture. Data are shown as the mean ± the s.d. ($^{**}P < 0.01$, $^*P < 0.05$).

iPS cell-derived myeloid cells might be caused by their apoptosis. In flow cytometric analysis, SCN-iPS cell-derived myeloid cells contained a significantly higher proportion of annexin V-positive cells than control iPS-derived myeloid cells on day 7 of culture, suggesting that the maturation arrest in myeloid cells derived from SCN-iPS cells might be caused by their apoptosis (Fig. 2*D*).

We next examined ELANE mRNA expression levels in nonadherent cells derived from SCN-iPS vs. control iPS cells (Fig. 2*E*). ELANE expression was significantly lower in nonadherent cells derived from SCN-iPS vs. control iPS cells on days 2 and 4 of culture ($P < 0.01$), as reported (16, 17). However, the former was a little higher than the latter on day 7 ($P < 0.01$). This result may be explained by the existence of SCN-iPS cell-derived myeloid cells arrested at an early stage along the neutrophil differentiation pathway even on day 7 of culture. We also examined the expression of proteinase 3 and azurocidin, which comprise a family of closely related genes encoding neutrophil granule proteins along with ELANE, and found these genes were more highly expressed on day 4 (Fig. S3).

It has been reported that induction of the endoplasmic reticulum stress (ER) response and the unfolded protein response (UPR) has been advanced as a potential explanation for the molecular pathogenesis of SCN (18, 19). Thus, we examined activation of the UPR by X-box binding protein 1 (XBP-1) mRNA splicing on day 7. As shown in Fig. 2*F*, SPN-iPS cells induced XBP-1 mRNA splicing. We also found the up-regulation of BiP

(also known as GRP78 or HSPA5) (Fig. 2*G*). These results suggested that ER stress response and UPR might be involved in the pathogenesis in SCN.

To examine further the differences in gene expression between the two cell types, a microarray analysis was carried out by using $CD34^+$ cells derived from SCN-iPS and control iPS cells (three clones of each) in suspension culture on day 2. At this early time point, differences in cell number and morphology were not yet readily discernible between SCN-iPS and control iPS cells, as shown in Fig. 2*A*. However, the microarray analysis revealed a differential expression of various genes between the two cell types. Transcription factor genes, which were related to neutrophil development [e.g., CCAAT/enhancer-binding protein (C/EBP)-α (20), C/EBP-β (21), C/EBP-ε (22), and SPI1 (also known as PU.1) (23)], were all down-regulated in SCN-iPS cells. B-cell chronic lymphocytic leukemia/lymphoma 2, which regulates cell death under ER stress through the core mitochondrial apoptosis pathway (24), was also down-regulated (Fig. 3*A*). These findings were confirmed by quantitative reverse-transcriptional PCR (qRT-PCR), as shown in Fig. 2*H*.

Notably, the down-regulation of the genes in SCN-iPS cells related to and regulated by the wingless-type mmtv integration site family, member 3a (Wnt3a)/β-catenin pathway [e.g., Wnt3a, lymphoid enhance-binding factor (LEF)-1, BIRC5 (also known as survivin), and cyclin D1] was also uncovered by microarray analysis and qRT-PCR (Fig. 3 *A–C* and Fig. S4). Therefore, we examined the effect of enhancement of Wnt3a/β-catenin signaling by exogenous Wnt3a addition on the neutrophil development of $CD34^+$ cells derived from SCN-iPS and control iPS cells. Although Wnt3a did not stimulate the survival, proliferation, and differentiation of $CD34^+$ cells derived from both iPS cells in the absence of cytokines stimulating myelopoiesis including G-CSF, the addition of Wnt3a to the neutrophil differentiation medium induced a dose-dependent increase in the percentage of mature neutrophils among the cultured cells, as shown in Fig. 3 *D* and *E*. Furthermore, when Wnt3a was added concurrently with 1,000ng/mL G-CSF, the proportion of mature neutrophils increased more than it did with Wnt3a or 1,000 ng/mL G-CSF alone, reaching a value comparable with that observed for control iPS cells (Fig. 4 *A* and *B*).

The reduced expression of LEF-1 (as regulated by the Wnt3a/β-catenin pathway) reportedly plays a critical role in the defective maturation of neutrophils in SCN patients (25). Therefore, we next examined LEF-1 mRNA expression in SCN-iPS–$CD34^+$ cells cultured in the presence of Wnt3a, G-CSF (1,000 ng/mL), or both. Wnt3a and G-CSF both enhanced LEF-1 mRNA expression, but the most significant increase was observed in the presence of Wnt3a plus G-CSF. LEF-1 expression in SCN-iPS–$CD34^+$ cells in response to Wnt3a plus G-CSF was almost the same as that in control iPS–$CD34^+$ cells (Fig. 4*C*). These results substantiate the importance of LEF-1 in neutrophil development and the pathogenesis of SCN, as shown (25). Moreover the

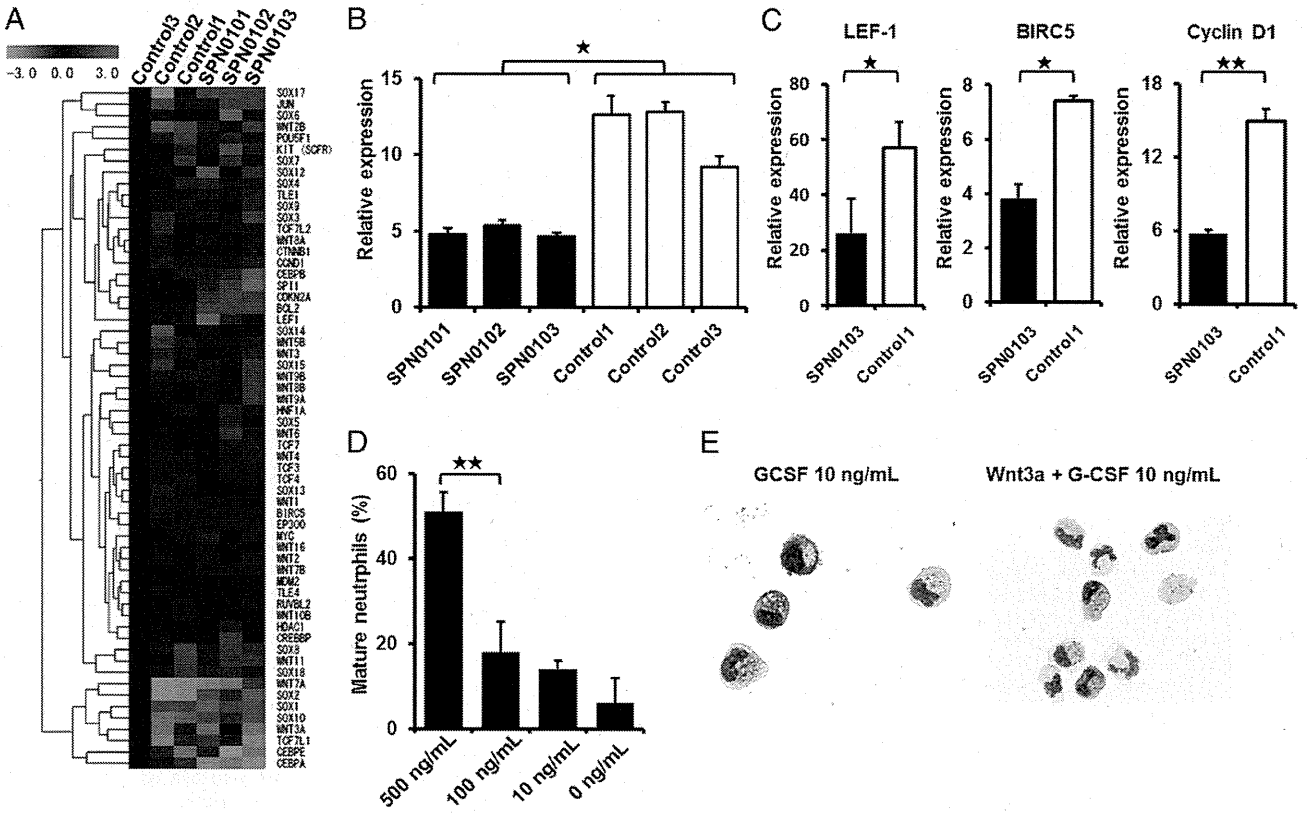

Fig. 3. Effects of Wnt3a on neutrophil development from SCN-iPS cells. (*A*) Heat map showing differential gene expression among SCN-iPS and control iPS cells on day 2. Red, high gene expression; blue, low gene expression compared with gene expression in control 3. (*B*) qRT-PCR analysis of the relative mRNA expression (target/HPRT expression) of Wnt3a on day 2. Filled and open bars indicate experiments using SCN-iPS cells (SPN0101, SPN0102, and SPN0103) and control iPS cells (controls 1, 2, and 3), respectively. Data are shown as mean ± SD. $^*P < 0.05$. (*C*) qRT-PCR analysis of the relative expression (target/HPRT expression) of genes regulated by the Wnt3a/β-catenin pathway (LEF-1, survivin, and cyclin D1) in SCN-iPS cells (filled bars, SPN0103) vs. control iPS cells (open bars, control 1) on day 2 of suspension culture. Data are shown as mean ± SD. $^{**}P < 0.01$; $^*P < 0.05$. (*D*) Proportion of mature neutrophils among the cells derived from SCN-iPS cells (SPN0102) on day 14 of suspension culture with dose escalation of Wnt3a. Data are shown as mean ± SD. $^{**}P < 0.01$. (*E*) Photographs of nonadherent cells on day 7 of suspension culture with or without Wnt3a (500 ng/mL) (400×; May–Grünwald–Giemsa staining).

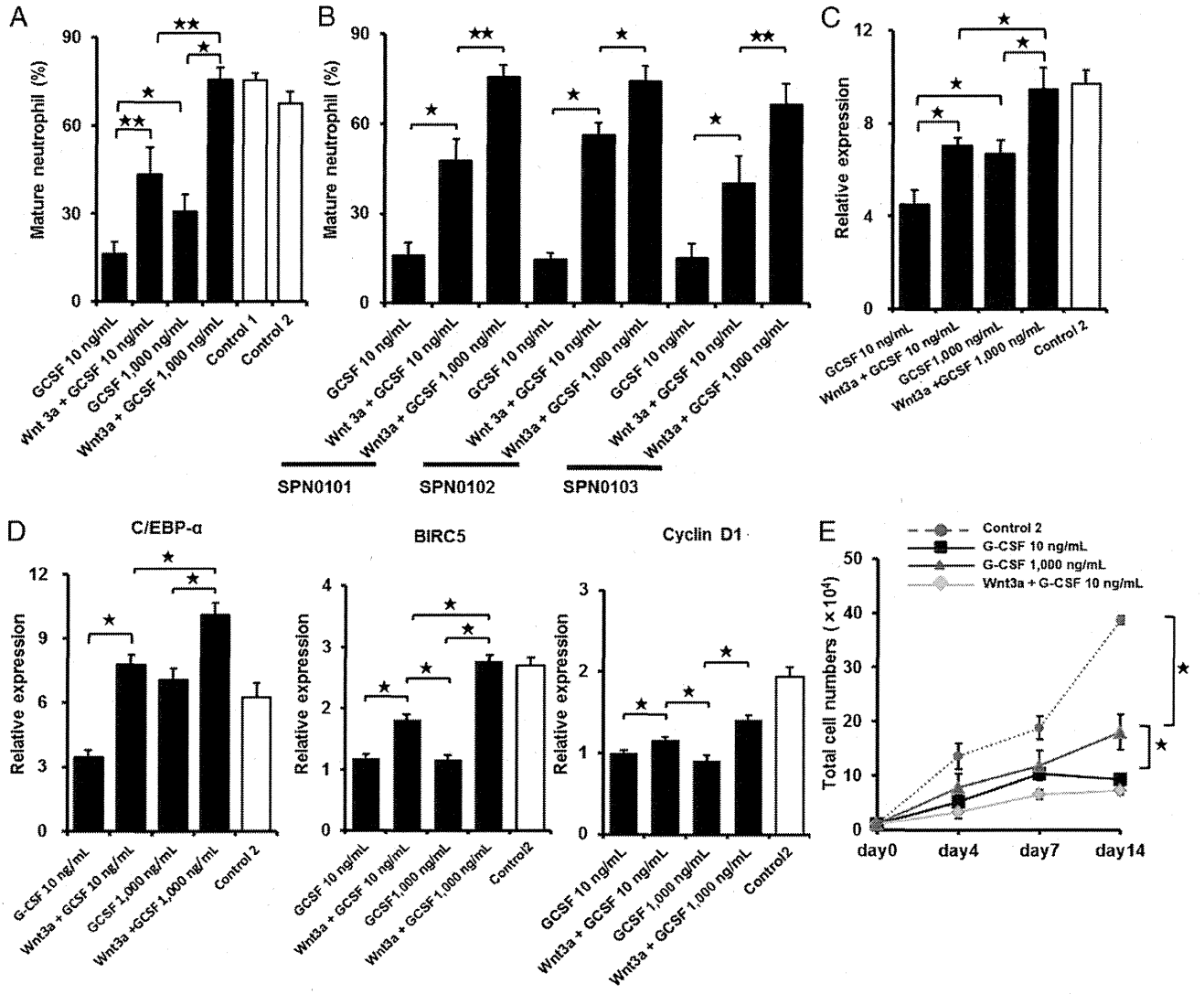

Fig. 4. Effects of Wnt3a in combination with high-dose G-CSF. (*A*) Filled and open bars show the proportion of mature neutrophils among the cells derived from SCN-iPS cells (SPN0101) on day 14 of suspension culture in the presence of neutrophil differentiation medium containing 10 ng/mL G-CSF (GCSF 10 ng/mL); 500 ng/mL Wnt3a and 10 ng/mL G-CSF (Wnt3a+GCSF 10 ng/mL); 1,000 ng/mL G-CSF (GCSF 1,000 ng/mL); or 500 ng/mL Wnt3a and 1,000 ng/mL G-CSF (Wnt3a + GCSF 1,000 ng/mL); and that from control iPS cells (controls 1 and 2) cultured in the neutrophil differentiation medium containing 10 ng/mL G-CSF, respectively. Data are shown as mean ± SD. $^{**}P < 0.01$; $^{*}P < 0.05$. (*B*) The proportion of mature neutrophils among the cells derived from three SCN-iPS cell clones (SPN0101, SPN0102, and SPN0103) on day 14 of suspension culture in the presence of neutrophil differentiation medium containing 10 ng/mL G-CSF (GCSF 10 ng/mL); 500 ng/mL Wnt3a and 10 ng/mL G-CSF (Wnt3a+GCSF 10 ng/mL); or 500 ng/mL Wnt3a and 1,000 ng/mL G-CSF (Wnt3a + GCSF 1,000 ng/mL). Data are shown as mean ± SD. $^{**}P < 0.01$; $^{*}P < 0.05$. (*C*) Filled and open bars show the relative expression (target/HPRT expression) of LEF-1 mRNA in SCN-iPS cells (SPN0101) on day 2 of suspension culture in the presence of differentiation medium containing the same combinations of Wnt3a and G-CSF as shown in *A* and that from control iPS cells (control 2), respectively. Data are shown as mean ± SD. $^{**}P < 0.01$; $^{*}P < 0.05$. (*D*) Filled and open bars show the relative expression (target/HPRT expression) of C/EBP-α, BIRC5, or cyclin D1 mRNA in SCN-iPS cells (SPN0101) on day 2 of suspension culture in the presence of differentiation medium containing the same combinations of Wnt3a and G-CSF as shown in *A* and that from control iPS cells (control 2), respectively. Data are shown as mean ± SD. $^{**}P < 0.01$; $^{*}P < 0.05$. (*E*) Total cell numbers of nonadherent cells in suspension cultures of 1×10^4 $CD34^+$ cells derived from control iPS cells (control 2; red broken line) and SCN-iPS cells (SPN0101) in the presence of neutrophil differentiation medium (black line) and those from SCN-iPS cells in the presence of neutrophil differentiation medium containing 500 ng/mL Wnt3a (yellow line) or 1,000 ng/mL G-CSF (black line). Data are shown as mean ± SD. $^{**}P < 0.05$.

administration of Wnt3a led to up-regulate C/EBP-α, cyclin D1, and BIRC5/survivin in addition to LEF-1 in the presence of G-CSF (Fig. 4*D*). These results suggested that the up-regulation of LEF-1 expression might promote granulopoiesis by increasing the expressions of cyclin D1, BIRC5/survivin, and C/EBP-α and its binding to LEF-1 in accordance with the previous report (25). Interestingly, Wnt3a did not stimulate the proliferation of myeloid cells, whereas 1,000 ng/mL G-CSF did to a certain extent (Fig. 4*E*). Hence, Wnt3a was capable of stimulating the maturation of impaired neutrophils in the presence of G-CSF, but not the proliferation of myeloid cells from SCN-iPS cells.

Importantly, aside from providing new insights into the mechanisms behind impaired neutrophil development in SCN patients, the present study demonstrates that agents activating the Wnt3a/β-catenin pathway are potential candidates for new drugs for SCN with mutations in the ELANE gene. Because endogenous G-CSF is readily increased in SCN patients (26), these activating agents may be viable alternatives to exogenous G-CSF treatment.

Materials and Methods

Additional information is available in *SI Materials and Methods*.

Generation of Human iPS Cells. BM fibroblasts from a patient with SCN and skin dermal fibroblasts from a healthy donor were acquired after obtaining informed consent after getting the approval by the Ethics Committee of the Institute of Medical Science, University of Tokyo, in accordance with the Declaration of Helsinki. The SCN patient presented with a heterozygous mutation in the ELANE gene in the 707 region of exon 5. SCN-iPS cells were established from the SCN-BM fibroblasts by transfection with the pMX retroviral vector, as described (10). This vector expressed the human transcription factors OCT3/4, SOX2, KLF4, and c-MYC. Control iPS cell clones, control 1 (TkDN4-M) and control 3 (201B7), were gifts from K. Eto and S. Yamanaka (Kyoto University, Kyoto), respectively (10, 11). Control 2 (SPH0101) was newly generated from another healthy donor's skin dermal fibroblasts by using the same methods.

Hematopoietic Colony Assay. A hematopoietic colony assay was performed in an aliquot of culture mixture, which contained 1.2% methylcellulose (Shin-Etsu Chemical), 30% (vol/vol) FBS, 1% (vol/vol) deionized fraction V BSA, 0.1 mM 2-mercaptoethanol (2-ME), α-minimum essential medium, and a cytokine mixture consisting of 100 ng/mL human stem cell factor (hSCF) (Wako), 100 ng/mL fusion protein 6 [FP6; a fusion protein of interleukin (IL)-6 and IL-6 receptor] (a gift from Tosoh), 10 ng/mL human IL-3 (hIL-3) (a gift from Kirin Brewery), 10 ng/mL human thrombopoietin (hTPO) (a gift from Kirin Brewery), 10 ng/mL human G-CSF (a gift from Chugai Pharmaceutical), and 5 U/mL human erythropoietin (a gift from Kirin Brewery). For dose escalation experiments, various concentrations (0, 1, 10, 100, and 1,000 ng/mL) of G-CSF were used instead of the cytokine mixture described above. Colony types were determined according to established criteria on day 14 of culture by in situ observations under an inverted microscope (IX70; Olympus) (27).

Suspension Culture and Neutrophil Differentiation Assay. $CD34^+$ cells (1×10^4 cells) were cocultured with irradiate confluent AGM-S3 cells in neutrophil differentiation medium containing Iscove's modified Dulbecco's medium, 10% FBS, 3 mM L-glutamine, 1×10^{-4} M 2-ME, 1×10^{-4} M nonessential amino acids solution, 100 ng/mL hSCF, 100 ng/mL FP6, 10 ng/mL hIL-3, 10 ng/mL hTPO, and 10 or 1,000 ng/mL human G-CSF. Wnt3a (10, 100, or 500 ng/mL) (R&D) was then added. The medium was replaced with an equivalent volume of fresh medium every 4 d. Living, nonadherent cells were counted following 0.4% trypan blue staining.

PCR primer. All primer sets used in this study are shown in Table S1.

Statistical Analysis. All data are presented as mean ± SD. $P < 0.05$ was considered significant. Statistical analyses were performed by using Prism software (GraphPad).

ACKNOWLEDGMENTS. We thank the individual with SCN who participated in this study; K. Eto for providing control iPS cells (control 1; TkDN4-M); S. Yamanaka for providing control iPS cells (control 3; 206B7); and E. Matsuzaka and S. Hanada for technical assistance. This work was supported by in part by Ministry of Education, Culture, Sports, Science, and Technology of Japan (MEXT) Grants-in-Aid (to Y.E.) and Project for Realization of Regenerative Medicine (MEXT) Grants-in-Aid (to K.Tsuji).

1. Zeidler C, Germeshausen M, Klein C, Welte K (2009) Clinical implications of *ELA2*-, *HAX1*-, and G-CSF-receptor (*CSF3R*) mutations in severe congenital neutropenia. *Br J Haematol* 144(4):459–467.
2. Freedman MH, et al. (2000) Myelodysplasia syndrome and acute myeloid leukemia in patients with congenital neutropenia receiving G-CSF therapy. *Blood* 96(2):429–436.
3. Dale DC, et al. (1993) A randomized controlled phase III trial of recombinant human granulocyte colony-stimulating factor (filgrastim) for treatment of severe chronic neutropenia. *Blood* 81(10):2496–2502.
4. Rosenberg PS, et al.; Severe Chronic Neutropenia International Registry (2006) The incidence of leukemia and mortality from sepsis in patients with severe congenital neutropenia receiving long-term G-CSF therapy. *Blood* 107(12):4628–4635.
5. Xia J, et al. (2009) Prevalence of mutations in ELANE, GFI1, HAX1, SBDS, WAS and G6PC3 in patients with severe congenital neutropenia. *Br J Haematol* 147(4):535–542.
6. Horwitz MS, et al. (2007) Neutrophil elastase in cyclic and severe congenital neutropenia. *Blood* 109(5):1817–1824.
7. Hajjar E, Broemstrup T, Kantari C, Witko-Sarsat V, Reuter N (2010) Structures of human proteinase 3 and neutrophil elastase—so similar yet so different. *FEBS J* 277(10): 2238–2254.
8. Fouret P, et al. (1989) Expression of the neutrophil elastase gene during human bone marrow cell differentiation. *J Exp Med* 169(3):833–845.
9. Pham CT (2006) Neutrophil serine proteases: Specific regulators of inflammation. *Nat Rev Immunol* 6(7):541–550.
10. Takayama N, et al. (2010) Transient activation of c-MYC expression is critical for efficient platelet generation from human induced pluripotent stem cells. *J Exp Med* 207(13):2817–2830.
11. Takahashi K, et al. (2007) Induction of pluripotent stem cells from adult human fibroblasts by defined factors. *Cell* 131(5):861–872.
12. Germeshausen M, Ballmaier M, Welte K (2007) Incidence of CSF3R mutations in severe congenital neutropenia and relevance for leukemogenesis: Results of a long-term survey. *Blood* 109(1):93–99.
13. Ma F, et al. (2007) Novel method for efficient production of multipotential hematopoietic progenitors from human embryonic stem cells. *Int J Hematol* 85(5):371–379.
14. Konishi N, et al. (1999) Defective proliferation of primitive myeloid progenitor cells in patients with severe congenital neutropenia. *Blood* 94(12):4077–4083.
15. Nakamura K, et al. (2000) Abnormalities of primitive myeloid progenitor cells expressing granulocyte colony-stimulating factor receptor in patients with severe congenital neutropenia. *Blood* 96(13):4366–4369.
16. Skokowa J, Fobiwe JP, Dan L, Thakur BK, Welte K (2009) Neutrophil elastase is severely down-regulated in severe congenital neutropenia independent of ELA2 or HAX1 mutations but dependent on LEF-1. *Blood* 114(14):3044–3051.
17. Kawaguchi H, et al. (2003) Dysregulation of transcriptions in primary granule constituents during myeloid proliferation and differentiation in patients with severe congenital neutropenia. *J Leukoc Biol* 73(2):225–234.
18. Köllner I, et al. (2006) Mutations in neutrophil elastase causing congenital neutropenia lead to cytoplasmic protein accumulation and induction of the unfolded protein response. *Blood* 108(2):493–500.
19. Grenda DS, et al. (2007) Mutations of the ELA2 gene found in patients with severe congenital neutropenia induce the unfolded protein response and cellular apoptosis. *Blood* 110(13):4179–4187.
20. Pabst T, et al. (2001) AML1-ETO downregulates the granulocytic differentiation factor C/EBPalpha in t(8;21) myeloid leukemia. *Nat Med* 7(4):444–451.
21. Hirai H, et al. (2006) C/EBPbeta is required for 'emergency' granulopoiesis. *Nat Immunol* 7(7):732–739.
22. Bedi R, Du J, Sharma AK, Gomes I, Ackerman SJ (2009) Human C/EBP-ε activator and repressor isoforms differentially reprogram myeloid lineage commitment and differentiation. *Blood* 113(2):317–327.
23. Friedman AD (2007) Transcriptional control of granulocyte and monocyte development. *Oncogene* 26(47):6816–6828.
24. Hetz C (2012) The unfolded protein response: Controlling cell fate decisions under ER stress and beyond. *Nat Rev Mol Cell Biol* 13(2):89–102.
25. Skokowa J, et al. (2006) LEF-1 is crucial for neutrophil granulocytopoiesis and its expression is severely reduced in congenital neutropenia. *Nat Med* 12(10):1191–1197.
26. Mempel K, Pietsch T, Menzel T, Zeidler C, Welte K (1991) Increased serum levels of granulocyte colony-stimulating factor in patients with severe congenital neutropenia. *Blood* 77(9):1919–1922.
27. Nakahata T, Ogawa M (1982) Hemopoietic colony-forming cells in umbilical cord blood with extensive capability to generate mono- and multipotential hemopoietic progenitors. *J Clin Invest* 70(6):1324–1328.

blood

2012 119: 5458-5466
Prepublished online April 19, 2012;
doi:10.1182/blood-2011-05-354167

Frequent somatic mosaicism of *NEMO* in T cells of patients with X-linked anhidrotic ectodermal dysplasia with immunodeficiency

Tomoki Kawai, Ryuta Nishikomori, Kazushi Izawa, Yuuki Murata, Naoko Tanaka, Hidemasa Sakai, Megumu Saito, Takahiro Yasumi, Yuki Takaoka, Tatsutoshi Nakahata, Tomoyuki Mizukami, Hiroyuki Nunoi, Yuki Kiyohara, Atsushi Yoden, Takuji Murata, Shinya Sasaki, Etsuro Ito, Hiroshi Akutagawa, Toshinao Kawai, Chihaya Imai, Satoshi Okada, Masao Kobayashi and Toshio Heike

Blood (print ISSN 0006-4971, online ISSN 1528-0020), is published weekly by the American Society of Hematology, 2021 L St, NW, Suite 900, Washington DC 20036.

Frequent somatic mosaicism of *NEMO* in T cells of patients with X-linked anhidrotic ectodermal dysplasia with immunodeficiency

Tomoki Kawai,[1] Ryuta Nishikomori,[1] Kazushi Izawa,[1] Yuuki Murata,[1] Naoko Tanaka,[1] Hidemasa Sakai,[1] Megumu Saito,[2] Takahiro Yasumi,[1] Yuki Takaoka,[1] Tatsutoshi Nakahata,[2] Tomoyuki Mizukami,[3] Hiroyuki Nunoi,[3] Yuki Kiyohara,[4] Atsushi Yoden,[5] Takuji Murata,[5] Shinya Sasaki,[6] Etsuro Ito,[6] Hiroshi Akutagawa,[7] Toshinao Kawai,[8] Chihaya Imai,[9] Satoshi Okada,[10] Masao Kobayashi,[10] and Toshio Heike[1]

[1]Department of Pediatrics, Kyoto University Graduate School of Medicine, Kyoto, Japan; [2]Clinical Application Department, Center for iPS Cell Research and Application, Institute for Integrated Cell-Material Sciences, Kyoto University, Kyoto, Japan; [3]Division of Pediatrics, Department of Reproductive and Developmental Medicine, Faculty of Medicine, University of Miyazaki, Miyazaki, Japan; [4]Department of Pediatrics, Faculty of Medicine, Osaka University, Suita, Japan; [5]Department of Pediatrics, Osaka Medical College, Takatsuki, Japan; [6]Department of Pediatrics, Hirosaki University Graduate School of Medicine, Hirosaki, Japan; [7]Department of Pediatrics, Kishiwada City Hospital, Kishiwada, Japan; [8]Department of Human Genetics, National Center for Child Health and Development, Tokyo, Japan; [9]Department of Pediatrics, Niigata University, Niigata, Japan; and [10]Department of Pediatrics, Hiroshima University Graduate School of Biomedical Sciences, Hiroshima, Japan

Somatic mosaicism has been described in several primary immunodeficiency diseases and causes modified phenotypes in affected patients. X-linked anhidrotic ectodermal dysplasia with immunodeficiency (XL-EDA-ID) is caused by hypomorphic mutations in the *NF-κB essential modulator (NEMO)* gene and manifests clinically in various ways. We have previously reported a case of XL-EDA-ID with somatic mosaicism caused by a duplication mutation of the *NEMO* gene, but the frequency of somatic mosaicism of *NEMO* and its clinical impact on XL-EDA-ID is not fully understood. In this study, somatic mosaicism of *NEMO* was evaluated in XL-EDA-ID patients in Japan. Cells expressing wild-type NEMO, most of which were derived from the T-cell lineage, were detected in 9 of 10 XL-EDA-ID patients. These data indicate that the frequency of somatic mosaicism of *NEMO* is high in XL-ED-ID patients and that the presence of somatic mosaicism of *NEMO* could have an impact on the diagnosis and treatment of XL-ED-ID patients. (*Blood.* 2012;119(23):5458-5466)

Introduction

X-linked anhidrotic ectodermal dysplasia with immunodeficiency (XL-EDA-ID) is a disease with clinical features including hypohidrosis, delayed eruption of teeth, coarse hair, and immunodeficiency associated with frequent bacterial infections.[1-5] The gene responsible for XL-EDA-ID has been identified as *NF-κB essential modulator (NEMO)*.[6-8] NEMO is necessary for the function of IκB kinase, which phosphorylates and degrades IκB to activate NF-κB.[9-10] Defects in NEMO cause various abnormalities in signal transduction pathways involving NF-κB, and affect factors such as the IL-1 family protein receptors, the TLRs, VEGFR-3, receptor activator of nuclear factor κB (RANK), the ectodysplasin-A receptor, CD40, and the TNF receptor I.[7] Whereas a complete loss of NEMO function in humans is believed to cause embryonic lethality,[11] *NEMO* mutations in XL-EDA-ID patients are hypomorphic,[8] causing a partial loss of NEMO functions.

In XL-EDA-ID, NEMO defects lead to diverse immunologic features including susceptibility to pathogens, impaired Ab response to polysaccharides,[2,4,12] hypogammaglobulinemia,[13] hyper IgM syndrome,[14] and impaired NK-cell activity,[15] with a large degree of variability in phenotypes among the patients. For example, approximately one-tenth of XL-EDA-ID patients exhibit reduced mitogen-induced proliferation of T lymphocytes.[12] Moreover, one-fourth suffer from inflammatory disorders such as inflammatory bowel disease and rheumatoid arthritis,[12] although the inflammatory process usually relies on NF-κB activation.[16] One explanation for this clinical variability is that the XL-EDA-ID phenotype is *NEMO* genotype-specific. Although the XL-EDA-ID database reported by Hanson et al succeeds to some extent in linking the specific clinical features to *NEMO* genotype,[12] the penetrance of some clinical features is not high and the mechanism accounting for this variability is unknown.

Recently, we have reported a case of spontaneous reversion mosaicism of the *NEMO* gene in XL-EDA-ID, which showed an atypical phenotype involving decreased mitogen-induced T-cell proliferation along with decreased CD4 T cells (patient 1).[17] There have been no subsequent reports on somatic mosaicism in XL-EDA-ID, and its prevalence and impact on the clinical features of the disease is unknown. In this study, we describe the younger brother of patient 1, who suffered from XL-EDA-ID with the same mutation and somatic reversion mosaicism of *NEMO*. Patient 2 showed intriguing laboratory findings in that mitogen-induced T-cell proliferation varied in accordance with the rate of detected reversion in the peripheral blood. These 2 cases led us to perform a nationwide study of XL-EDA-ID patients in Japan that revealed a high incidence of somatic mosaicism of *NEMO*.

Submitted May 11, 2011; accepted April 8, 2012. Prepublished online as *Blood* First Edition paper, April 19, 2012; DOI 10.1182/blood-2011-05-354167.

The online version of this article contains a data supplement.

The publication costs of this article were defrayed in part by page charge payment. Therefore, and solely to indicate this fact, this article is hereby marked "advertisement" in accordance with 18 USC section 1734.

Table 1. Clinical and genetic features of XL-EDA-ID patients

Patient	Mutation	Ectodermal dysplasia	Mitogen-induced proliferation	Infections	Complications	Therapy	Sex chromosome chimerism
1	Duplication	+	Reduced	Sepsis (S.P. and P.A.)	Chronic diarrhea	IVIG	100% XY
				Disseminated M.A.C.	Failure to thrive	RFP, CAM, AMK, EB	
				Skin abscess (S.A.)	Small intestinal stenosis	Rifabutin	
				Invasive *Aspergillus*	Lymphedema		
2	Duplication	+	Reduced	Sepsis (*E coli*)	Failure to thrive	IVIG, ST, EB, CAM	99.8% XY 0.2% X
				Disseminated M.S.		Rifabutin, SCT	
3	D311E	−	Normal	Disseminated B.C.G.		IVIG, INH	100% XY
				Sepsis (S.P.)		RFP, SCT	
4	A169P	+	Normal	Meningitis (S.P.)	IBD	IVIG, ST, PSL	99% XY
					Interstitial pneumonia	CyA, MTX, Infliximab	
					Rheumatoid arthritis		
5	L227P	+	Normal	Recurrent pneumonia	IBD	ST, mesalazine	Not done
				Pyogenic coxitis		Infliximab	
				Recurrent otitis media			
6	R182P	+	Not done	Recurrent otitis media	IBD	ST, mesalazine	99.8% XY 0.2% X
				UTI, Recurrent stomatitis			
				Subepidermal abscess			
7	R175P	+	Normal	Recurrent sepsis (S.P.)		IVIG	100% XY
8	Q348X	+	Normal	Disseminated B.C.G.	IBD	IVIG, ST	100% XY
9	R175P	+	Normal	Recurrent pneumonia	IBD	IVIG	100% XY
				Recurrent otitis media		5-aminosalicylic acid	
				Kaposi varicelliform eruption			
10	1167 ins C	+	Normal	Sepsis and Enteritis (E.A)	Failure to thrive	IVIG, SCT	Not done
				Sepsis (C.G.)	Pyloric stenosis, colon polyps		
				UTI (K.P.)			

S.P. indicates *Streptococcus pneumoniae*; P.A., *Pseudomonas aeruginosa*; IVIG, intravascular immunoglobulin infusion; M.A.C., *Mycobacterium avium* complex; S.A., *Staphylococcus aureus*; *E coli*, *Escherichia coli*; ST, trimethoprim-sulfamethoxazole; M.S., *Mycobacterium szulgai*; AMK, amikacin; EB, ethambutol; CAM, clarithromycin; SCT, stem cell transplantation; B.C.G., Bacille de Calmette et Guerin; INH, isoniazid; RFP, rifampicin; IBD, inflammatory bowel disease; PSL, prednisolone; CyA, cyclosporine A; MTX, methotrexate; UTI, urinary tract infection; E.A., *Enterobacter aerogenes*; C.G., *Candida glabrata*; and K.P., *Klebsiella* pneumonia.

Methods

Informed consent

Informed consent was obtained from the patients and their families following the Declaration of Helsinki according to the protocol of the Internal Review Board of Kyoto University, which approved this study.

Patients

Patient 1 was an XL-EDA-ID patient with a duplication mutation of the *NEMO* gene spanning intron 3 to exon 6. This patient has been reported previously[17] and died from an *Aspergillus* infection at the age of 4. Patient 2, born at term, was the younger brother of patient 1. This patient was also diagnosed as XL-EDA-ID with the same duplication mutation as patient 1 by genetic study. He received trimethoprim-sulfamethoxazole prophylaxis and a monthly infusion of immunoglobulin from the age of 1 month. The patient maintained good health and had a body weight of 7899*g* at 6 months when he started to fail to thrive. Except for poor weight gain, patient 2 appeared active with a good appetite, negative C-reactive protein, normal white blood cell counts, and no apparent symptoms. At 19 months of age, *Mycobacterium szulgai* was detected by venous blood culture, and the patient was treated with multidrug regimens including ethambutol, rifabutin, and clarithromycin based on the treatment of systemic *Mycobacterium avium* complex infection. The patient responded well to the treatment and his weight increased from 7830*g* to 9165*g* within a month after the treatment was initiated. Patient 2 received an unrelated cord blood cell transplantation at 26 months of age, containing 8.5×10^7 nucleated cells/kg (4.4×10^5 $CD34^+$ cells/kg), which was matched at 5 of 8 loci: mismatches occurred at 1 HLA-B and 1 HLA-C allele (according to serology), and at 1 HLA-A, 1 HLA-B, and 1 HLA-C allele (according to DNA typing). The preconditioning regimen consisted of fludarabine (30 mg/m^2/d) on days −7 to −3, melphalan (70 mg/m^2/d) on days −6 to −5, and rabbit anti-thymocyte globulin (2.5 mg/kg/d) on days −6 to −2. At first, Tacrolimus (0.024 mg/kg/d) was used to prevent GVHD, but this was switched to cyclosporin A (3 mg/kg/d) on day 9 because of drug-induced encephalopathy. Neutrophil ($> 0.5 \times 10^9$/L) and platelet ($> 50 \times 10^9$/L) engraftment were examined on days 13 and 40, respectively. Although $CD19^+$ cells (2042/μL, 94% donor chimerism), $CD56^+$ cells (242/μL, 97% donor chimerism), and monocytes (557/μL, 69% donor chimerism) were successfully generated, $CD3^+$ cells were not detected in the peripheral blood by day 54. The patient suffered from septic shock and died on day 60. Patients 3 to 10 were XL-EDA-ID patients recruited nationwide in Japan. Clinical details of patients 3, 4, and 10 have been reported previously.[18-20] These patients had clinical phenotypes characteristic of XL-EDA-ID such as ectodermal dysplasia, innate and/or acquired immunity defects, and susceptibility to pyogenic bacteria and *Mycobacterium* infection. Every patient had a mutation in the *NEMO* gene that caused reduced NF-κB activation in a NEMO reconstitution assay, as described in "Proliferation of $NEMO^{normal}$ and $NEMO^{low}$ T cells." Patient profiles are listed in Table 1.

Flow cytometric analysis

NEMO intracellular staining was performed as previously described.[17] The cells were stained for the following lineage markers before staining for NEMO: CD4, CD8, CD14, CD15, CD19, CD56, CD45RA (BD Biosciences/BD Pharmingen), and CCR7 (R&D Systems Inc). Intracellular staining of human IFN-γ, TNF-α, and NEMO was performed as previously described.[18] The stained cells were collected using a FACSCalibur flow cytometer (BD Biosciences) and analyzed using the FlowJo software (TreeStar).

Reporter assay

Wild-type and mutant *NEMO* cDNAs were generated from a healthy volunteer and the recruited XL-EDA-ID patients by RT-PCR; the cDNAs were subcloned into the p3xFLAG-CMV14 vector (Sigma-Aldrich). NEMO null rat fibroblast cells (kindly provided by Dr S. Yamaoka, Department of Molecular Virology, Graduate School of Medicine, Tokyo Medical and Dental University, Tokyo, Japan) were plated at a density of

3×10^4 cells/well in a 24-well culture dish and were transfected with 40 ng of NF-κB reporter plasmid (pNF-κB-Luc; BD Biosciences/BD Clontech), 2 ng of *NEMO* mutant expression construct, 10 ng of internal control for the normalization of transfection efficiency (pRL-TK; Toyo Ink), and 148 ng of mock vector using FuGENE HD Transfection Reagent (TOYO-B-Net) according to the manufacturer's protocol. Twelve hours after transfection, the cells were stimulated with 15 ng/mL lipopolysaccharide (LPS; Sigma-Aldrich) for 4 hours and the NF-κB activity was measured using the PicaGene Dual SeaPansy assay kit (TOYO-B-Net). Experiments were performed in triplicate and firefly luciferase activity was normalized to *Renilla* luciferase activity.

Subcloning analysis of cDNA

Cell sorting of the various cell lineages was performed by FACSVantage (BD Biosciences). The purity of each lineage was > 95%. The cDNA from sorted cells was purified and reverse transcribed by Super Script III (Invitrogen) with random hexamers and amplified by the proofreading PCR enzyme KOD, as previously described.[17,21] The PCR primers used were NEMO2 (5′-AGAGACGAAGGAGCACAAAGCTGCCTTGAG-3′) and NEMO3 (5′-ACTGCAGGGACAATGGTGGGTGCATCTGTC-3′). The PCR products were subcloned using a TA cloning kit (Invitrogen) and sequenced by ABI 3130xl Genetic analyzer (Applied Biosystems). To determine whether additional mutations occurred in revertant subclones that had wild-type sequence in the original mutation site, the entire coding region of the *NEMO* gene was sequenced and an additional mutation was considered present when the same mutation was detected in multiple subclones.

Allele-specific PCR

The mRNA purified from sorted T cells and monocytes was reverse-transcribed by SuperScript III (Invitrogen) with the gene-specific primer NEMO2 and amplified by the proofreading PCR enzyme KOD (Toyobo) using the primers NEMO3 and NEMO 4 (5′-TGTGGACACGCAGTGAAACGTGGTCTGGAG-3′). The PCR products were used as templates for allele-specific PCRs with Ex Taq polymerase (Takara Bio). Mutant and wild-type *NEMO* DNA was generated from each NEMO expression plasmid, mixed at graded ratios, and used as controls. PCR conditions and primer sequences are listed in supplemental Table 1 (available on the *Blood* Web site; see the Supplemental Materials link at the top of the online article).

Proliferation of NEMO^{normal} and NEMO^{low} T cells

To obtain PHA-induced T-cell blasts, PBMCs were stimulated with PHA (1:100; Invitrogen) and cultured in RPMI 1640 supplemented with 5% FCS and recombinant human IL-2 (50 IU/mL; kindly provided by Takeda Pharmaceutical Company) at 37°C for 7 days. Subcloning analysis of the cDNA obtained from the T-cell blasts was performed as described in "Subcloning analysis of cDNA."

Results

Reversion mosaicism of NEMO occurred in siblings with similar immunologic phenotypes

We previously reported patient 1 with a duplication mutation of the *NEMO* gene spanning intron 3 to exon 6, who was diagnosed as XL-EDA-ID at 1 year of age after suffering from recurrent infections.[17] At first, genetic diagnosis of the patient was difficult because the expression of aberrant *NEMO* mRNA was masked by the expression of normal *NEMO* mRNA by the revertant cells. Flow cytometric analysis of intracellular NEMO expression revealed cells with normal (NEMO^{normal}) and reduced (NEMO^{low}) levels of NEMO expression, indicating the presence of reversion mosaicism of the *NEMO* gene, and further analysis revealed that the *NEMO* mutation was disease-causing. PCR across the mutated region and sequencing of the PCR products revealed a duplication extending from intron 3 to exon 6, which was confirmed by Southern blot analysis. Additional copy number analysis of the *NEMO* gene of patient 1 and his mother excluded the possibility of a complex chromosomal aberration such as multiple duplication of the *NEMO* gene (supplemental Figure 1). Furthermore, polymorphism analysis using variable number tandem repeats on NEMO^{normal} and NEMO^{low} cells from patient 1 revealed that these cells were derived from the same origin (supplemental Table 2), indicating that the *NEMO* gene mosaicism was less likely because of amalgamation. The genomic analysis of the NEMO^{normal} cells revealed a complete reversion of the *NEMO* gene with no additional mutations. The clinical phenotype of patient 1 was combined immunodeficiency with a reduced number of T cells and mitogen-induced proliferation (Tables 2-3). We previously determined that reduced NEMO expression in the mutant T cells caused impairment of T-cell development and mitogen-induced proliferation.

Patient 2, the younger brother of patient 1, was diagnosed as XL-EDA-ID with the same duplication mutation as his brother. Flow cytometric analysis of intracellular NEMO expression performed at diagnosis showed that most of his PBMCs had reduced NEMO expression (Figure 1A). At 2 months of age, when most of the T cells were NEMO^{low}, absolute counts of the patient's T cells and the mitogen-induced proliferation of the patient's PBMCs were comparable with those of the healthy controls (Figure 1A-B; Table 2). These findings indicated that the *NEMO* mutation had no effect on T-cell development and mitogen-induced proliferation during early infancy in patient 2.

NEMO^{normal} T cells gradually increased as patient 2 grew older, while the absolute count of NEMO^{low} T cells decreased (Figure 1A-B). Accordingly, normal full-length *NEMO* cDNA, which had been undetectable in cord blood, was detectable in the patient's peripheral blood at 12 months of age. However, while NEMO^{normal} T cells were increasing, mitogen-induced T-cell proliferation started to decrease (Table 3), and the patient started to show poor weight gain from 6 months of age. When patient 2 was 17 months old, a blood culture revealed an *M szulgai* bacteremia. At this time, the absolute count of NEMO^{normal} T cells peaked, and NEMO^{low} T cells were at a minimum. He began to gain weight after anti-*Mycobacterium* medication was initiated, although NEMO^{normal} T cells started to decrease and NEMO^{low} T cells began to increase (Figure 1B). When the patient was 23 months old, mitogen-induced T-cell proliferation was still low and a roughly equal number of NEMO^{low} and NEMO^{normal} T cells were detected (Table 3). Overall, as patient 2 grew older, NEMO^{normal} T cells increased as the total number of T cells and the mitogen-induced T-cell proliferation decreased, similar to what had occurred in patient 1 at a similar age.

Various analyses were performed to compare the immunologic phenotype of NEMO^{low} and NEMO^{normal} T cells in detail. Both NEMO^{normal} and NEMO^{low} CD4$^+$ T cells carried a diverse Vβ repertoire, but CD8$^+$ T cells had a skewed Vβ repertoire regardless of NEMO expression level (Figure 1C). Surface marker analysis revealed that most of the NEMO^{normal} T cells were CD45RA$^-$/CCR7$^-$ and most of the NEMO^{low} T cells were CD45RA$^+$/CCR7$^+$ (Figure 1D). The NEMO^{normal} T cells produced similar amounts of IFN-γ and TNF-α as healthy control cells, while the production of these cytokines were reduced in NEMO^{low} T cells (Figure 1E-F). Taken together, these data implied that the immunologic phenotype of T cells from patient 2 converged with that of patient 1 as patient 2 grew older.

Table 2. Surface marker analysis of peripheral mononuclear cells of patients 1 and 2

	Patient 1	Patient 2		Healthy controls
Age at analysis	2 y	2 mo	19 mo	
CD3	1503	2366	1014	2997 ± 1751
CD4	292	1583	374	1683 ± 874
CD8	1160	783	547	1114 ± 976
TCRαβ	1386	2295	439	2620 ± 1612
TCRγδ	109	74	574	343 ± 177
$CD4^+CD45RA$	58	1336	105	1471 ± 890
$CD4^+CD45RO$	263	307	266	497 ± 189
$CD8^+CD45RA$	1178	783	297	1083 ± 1078
$CD8^+CD45RO$	361	21	250	385 ± 442
$CD4^+CD25$	80	427	93	210 ± 99
CD19	1200	941	1543	1252 ± 1145
CD20	1189	931	1536	1125 ± 837
$CD19^+$Sm-IgG	7	18	17	54 ± 21
$CD19^+$Sm-IgA	15	4	14	18 ± 14
$CD19^+$Sm-IgM	1171	910	1505	1057 ± 881
$CD19^+$Sm-IgD	1171	906	1495	1052 ± 884
CD16	912	176	24	287 ± 200
CD56	908	176	24	306 ± 207

Surface markers expressed by XL-EDA-ID patients' PBMCs are shown as absolute counts per microliter of peripheral blood. Healthy control values are based on children aged 1 to 6 years and are shown as the mean ± SD.

Sm indicates the surface membrane.

High incidence of somatic mosaicism of the *NEMO* gene in XL-EDA-ID patients

It is worth noting that somatic reversion mosaicism of the *NEMO* gene occurred in both of the 2 XL-EDA-ID siblings carrying a duplication mutation. To determine whether a high frequency of reversion is a specific event for this type of *NEMO* duplication mutation[22-25] or if the reversion of the *NEMO* gene occurs commonly in XL-EDA-ID patients, we recruited an additional 8 XL-EDA-ID patients from throughout Japan (Table 1) and analyzed the presence of *NEMO* reversion. These patients had various combinations of clinical phenotypes characteristic of XL-EDA-ID such as ectodermal dysplasia, innate and acquired immunity defects, and susceptibility to pyogenic bacteria and *Mycobacterium* infections. Every patient had a mutation of the *NEMO* gene with reduced NF-κB activation potential, as evaluated in a NEMO reconstitution assay (Figure 2).

Among the 8 patients, only patient 3 had a large proportion of $NEMO^{low}$ cells by flow cytometric analysis. The majority of patient 3's PBMCs were $NEMO^{low}$, whereas 10% of the patient's $CD8^+$ cells were $NEMO^{normal}$ (Figure 3A). This patient was identified as carrying the D311E mutation. Because missense mutations of the *NEMO* gene often do not result in the reduced expression of NEMO protein, subcloning and sequencing analysis was performed on the *NEMO* cDNA isolated from the remaining patients, and 6 of the 7 patients had normal *NEMO* subclones (Table 3). Expansion of maternal cells after fetomaternal transfusion was ruled out in these patients by FISH analysis with X and Y probes (Table 1).

Additional genetic analysis of the entire coding region of the *NEMO* gene was performed on $NEMO^{normal}$ cells from patient 3 and on reverted subclones from the other patients, except for patient 10 who had already received stem cell transplantation. The *NEMO* gene in these samples had reverted to wild-type with no additional mutations (Figure 3B and data not shown). To specifically determine in which cell lineages the reversion occurred, subcloning and sequencing analysis of cDNA in various cell lineages was performed. This analysis revealed that all the revertant cells were of the T-cell lineage and that no reversion occurred in monocytes and very little occurred in B cells (Table 4). Allele-specific PCR confirmed that reversion occurred in T cells but not in monocytes (Figure 4).

Selective advantage of $NEMO^{normal}$ cells in XL-EDA-ID carriers

The high frequency of somatic mosaicism in T cells of XL-EDA-ID patients indicated a strong selective advantage of wild-type NEMO T cells over T cells carrying mutant NEMO. To confirm this hypothesis, *NEMO* cDNA analysis was performed on various cell lineages from the mothers of the patients who are heterozygous for *NEMO* mutation and thus have mosaicism

Table 3. Immunologic analysis of patients 1 and 2

	Patient 1	Patient 2 (treated with IVIG)	
Age at analysis, mo	9	9	20
Serum immunoglobulin levels, g/L (control)			
IgG	10.63 (4.51-10.46)	8.44 (4.51-10.46)	10.37 (7.15-9.07)
IgA	1.36 (0.14-0.64)	1.88 (0.14-0.64)	3.93 (0.22-1.44)
IgM	0.4 (0.33-1.00)	0.17 (0.33-1.00)	0.20 (0.34-1.28)
Age at analysis	2 y	2 mo	23 mo
T-cell proliferation, SI (control)	9.3 (206.9 ± 142.5)	55.3 (64.8 ± 8.1)	7.2 (89.4 ± 31.2)

Control values of serum immunoglobulin levels are based on children aged either 7 to 9 months or 1 to 2 years and are shown as the mean ± SD. The T-cell proliferation assay was performed as described previously[17] with at least three healthy adults as controls.

SI indicates stimulation index; and IVIG, 2.5 g of monthly IV immune globulin infusion.

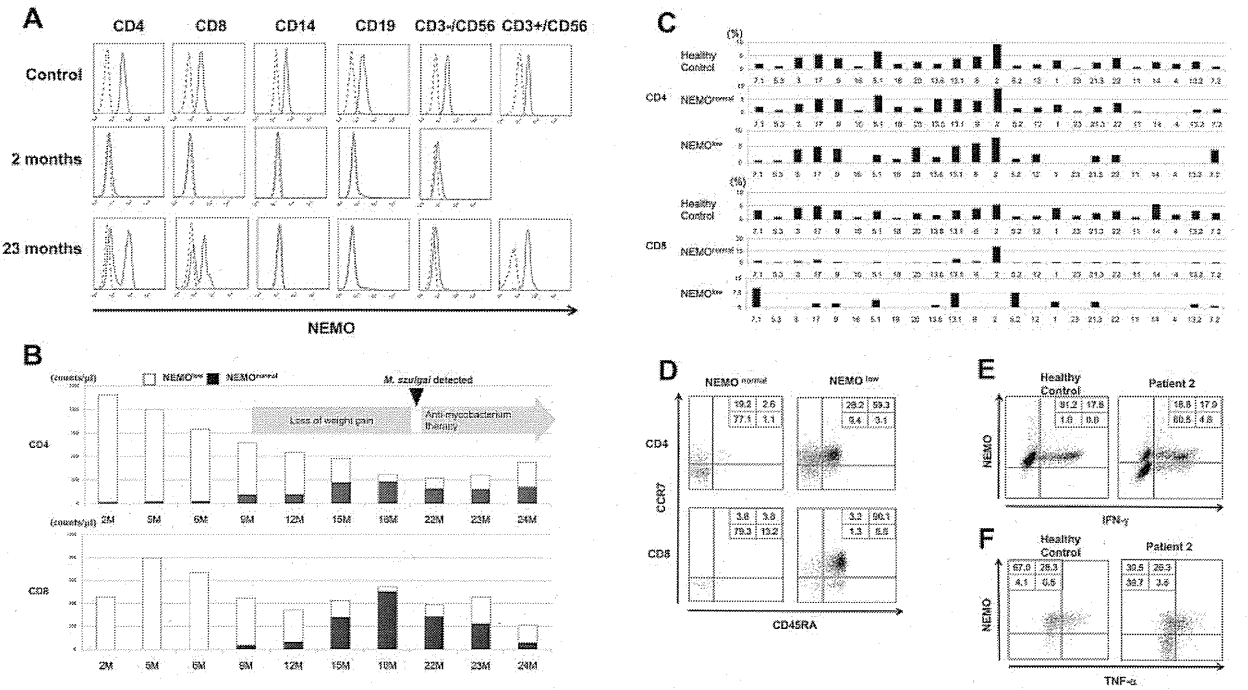

Figure 1. Identification and characterization of *NEMO* revertant T cells in patient 2. (A) Intracellular expression of NEMO in various PBMC lineages from a healthy adult control and patient 2 were evaluated by flow cytometry. For the patient, results of the analyses performed at 2 months and 23 months are shown. Solid lines indicate staining with the anti-NEMO mAb, and dotted lines indicate the isotype control. (B) Time-course variations in the absolute count of $NEMO^{normal}$ and $NEMO^{low}$ T cells in patient 2. M indicates age in months. (C) TCR-Vβ repertoire analysis of the patient's $CD4^+$ and $CD8^+$ T cells. PBMCs from the patient and a healthy adult control were stained for the TCR-Vβ panel, CD4, CD8, and NEMO, and analyzed by flow cytometry. (D) Phenotype analysis of T cells in patient 2. PBMCs from the patient and a control were stained for the expression of NEMO, CCR7, CD45RA, and CD4 or CD8. Data shown were gated on $NEMO^{normal}$ or $NEMO^{low}$ $CD4^+$ or $CD8^+$ cells. (E-F) Cytokine production from $NEMO^{normal}$ and $NEMO^{low}$ T cells. PBMCs from the patient and a control were stimulated with PMA and ionomycin for 6 hours and stained for intracellular (E) IFN-γ or (F) TNF-α along with NEMO. Cells shown are gated on the $CD3^+$ population.

because of X-chromosome inactivation. This analysis assumes that the percentage of cDNA for wild-type *NEMO* reflects the percentage of cells expressing wild-type NEMO. A high proportion of wild-type *NEMO* cDNA was observed in T cells from the mothers of patients 1/2, 3, 8, and 10, although wild-type *NEMO* cDNA was not predominant in T cells from the mother of patient 4 (Table 5).

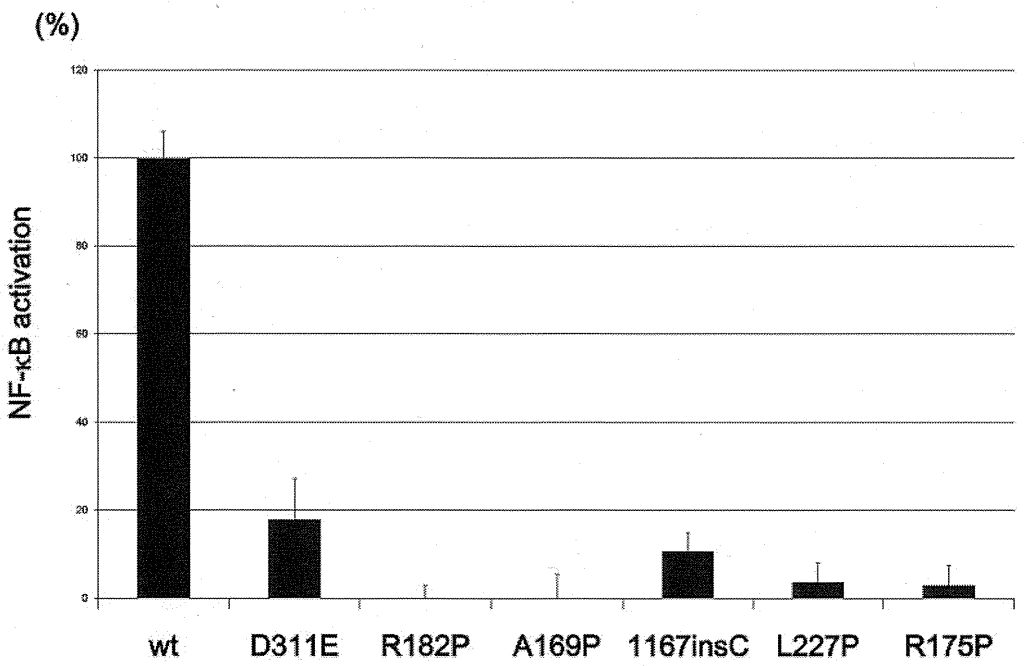

Figure 2. NF-κB transactivation by NEMO mutants from the XL-EDA-ID patients. NF-κB transactivation induced by NEMO mutants in the XL-EDA-ID patients. Mock vectors and wild-type (wt) NEMO were used as controls. The NF-κB activation index of NEMO variants were calculated as (NF-κB activation by each NEMO variant − NF-κB activation of the mock vector)/(NF-κB activation by wild-type NEMO − NF-κB activation of the mock vector). The data shown are the mean ± SD of triplicate wells and are representative of 3 independent experiments with similar results.

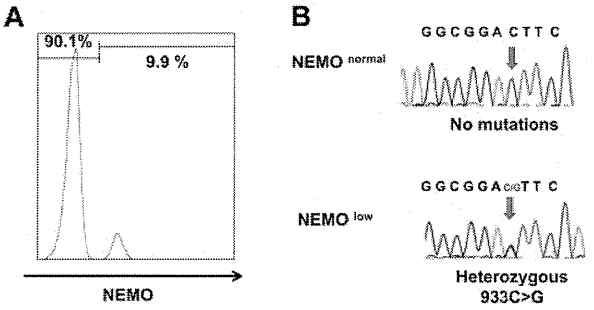

Figure 3. *NEMO* revertant T cells in patient 3. (A) Intracellular expression of NEMO in $CD8^+$ cells from patient 3. (B) Sequencing chromatograms of DNA from $NEMO^{normal}$ or $NEMO^{low}$ $CD8^+$ cells of patient 3. Arrows indicate the mutated base position at c. 931.

Similarly, there was an apparent high proportion of wild-type *NEMO* cDNA in monocytes and B cells from the mothers of patients 1/2, 8, and 10 (Table 5). These findings suggested a general selective advantage of $NEMO^{normal}$ cells over $NEMO^{low}$ cells in vivo, especially in T cells.

Proliferation capacity of $NEMO^{normal}$ and $NEMO^{low}$ T cells

T-cell proliferation stimulated by mitogens such as PHA is usually not reduced in XL-EDA-ID patients. However, the emergence of $NEMO^{normal}$ cells coincided with a reduction in mitogen-induced proliferation in patient 2. To further determine the effect of $NEMO^{normal}$ cells on mitogen-induced proliferation of peripheral T cells, the proportions of T cells carrying the wild-type and mutant were examined before and after PHA stimulation in XL-EDA-ID patients and their mothers (Table 6). In patients 2, 4, and 8, the percentage of the $NEMO^{normal}$ cells decreased after PHA stimulation, while $NEMO^{normal}$ cells prevailed in patient 9. In the mothers of patient 4 and 10, the percentage of $NEMO^{normal}$ cells increased after PHA stimulation, while the percentage of the $NEMO^{normal}$ cells decreased in the mother of patient 3. These results indicated that the NEMO mutation does not directly affect the mitogen-induced proliferation capacity of T cells and factors other than the *NEMO* genotype determine the proliferation capacity of $NEMO^{normal}$ and $NEMO^{low}$ T cells.

Discussion

Somatic reversion mosaicism has been described in several disorders affecting the hematopoietic system, the liver, and the skin.[23,26] Reports of somatic reversion cases have been particularly abundant in patients with immunodeficiency diseases, including Wiskott-Aldrich syndrome (WAS)[27] and SCID, which occur because of mutations in the interleukin receptor common γ chain,[28] CD3ζ,[29] *RAG-1*[30], and *ADA* genes.[31] Patients with somatic reversion mosaicism may present with significantly milder clinical phenotypes compared with nonrevertant patients with the same germline mutation, although this is not always the case.[26] One common feature in most cases where the somatic reversion mosaicism has been observed is a strong in vivo selective advantage of the revertant cells that express the wild-type gene product. One of the most intensively investigated diseases associated with somatic reversion mosaicism is WAS.[32-34] A report showed that up to 11% of WAS patients have presented with somatic reversion mosaicism.[33]

In our investigation, 9 of 10 XL-EDA-ID patients presented with somatic mosaicism. Two of the 9 were cases of reversion from a duplication mutation, while the others exhibited true back-reversion from a substitution or insertion mutation. This finding calls for caution when diagnosing XL-EDA-ID patients. Because the existence of a *NEMO* pseudogene makes it difficult to perform genetic analysis using genomic DNA, diagnosis of the disease is often confirmed by sequencing analysis of *NEMO* cDNA, and the presence of somatic mosaicism can cause misdiagnosis of XL-EDA-ID patients either when $NEMO^{normal}$ cells make up the majority of the patients' PBMCs or when the cDNA of the mutated *NEMO* gene cannot be amplified by PCR.[17] In fact, mutated *NEMO* cDNA could not be amplified from the PBMCs of patient 2 even when $NEMO^{normal}$ cells were absent (during early infancy), and only wild-type *NEMO* cDNA was amplified after the appearance of $NEMO^{normal}$ cells (data not shown), probably because of the instability of the mutated *NEMO* mRNA. Flow cytometric analysis of intracellular NEMO protein is of help in identifying the $NEMO^{low}$ cells in some patients, but the technique is not applicable when the *NEMO* mutation does not cause reduced expression of NEMO protein. Thus, some cases of XL-EDA-ID patients with reversion may be difficult to diagnose.

The high frequency of somatic mosaicism observed in XL-EDA-ID patients indicates a strong in vivo selective advantage for $NEMO^{normal}$ cells, which express the wild-type gene product. Patient 2 presented with a high mutant T-cell count at birth that gradually decreased over time (Figure 1B). This finding indicates that wild-type NEMO expression is critical for the survival of certain cell lineages, including T cells, after birth. On the other hand, no $NEMO^{normal}$ monocytes and very few $NEMO^{normal}$ B cells were detected in the recruited XL-EDA-ID patients (Table 4). This specific feature is similar to other somatic reversion mosaicism seen in primary immunodeficiency patients[26] and indicates that the expression of NEMO is less critical for the survival of monocytes or B cells compared with that of T cells. There is also an apparent

Table 4. Analysis of *NEMO* gene mosaicism in various cell lineages for each patient

Patient	Mutation	Age at analysis	CD4, % (proportion)	CD8, % (proportion)	CD14, % (proportion)	CD19, % (proportion)
1	Duplication	2 y	90	100	0	4.0
2	Duplication	15 mo	45	66	0	4.0
3	D311E	3 y	2.4	9.9	0	1.2
4	A169P	12 y	0 (0/19)	24 (9/37)	0 (0/19)	0 (0/47)
5	L227P	3 y	0 (0/25)	0 (0/35)	0 (0/30)	0 (0/25)
6	R182P	4 y	18 (5/28)	17 (9/52)	0 (0/27)	0 (0/33)
7	R175P	6 y	0.4 (1/25)	39 (11/28)	0 (0/28)	0 (0/25)
8	Q348X	8 y	38 (6/16)	47 (9/19)	0 (0/33)	0 (0/25)
9	R175P	15 y	30 (9/30)	36 (12/33)	0 (0/23)	0 (0/14)
10	1167 ins C	9 mo	PBMC 9.3 (4/43)			

For patients 1 to 3, data represent the percentages of $NEMO^{normal}$ cells in each lineage, as assessed by flow cytometry. For patients 4 to 10, the ratio indicates the number of wild-type NEMO clones in various cell lineages as compared with the total number of clones analyzed, based on subcloning and sequencing analysis.

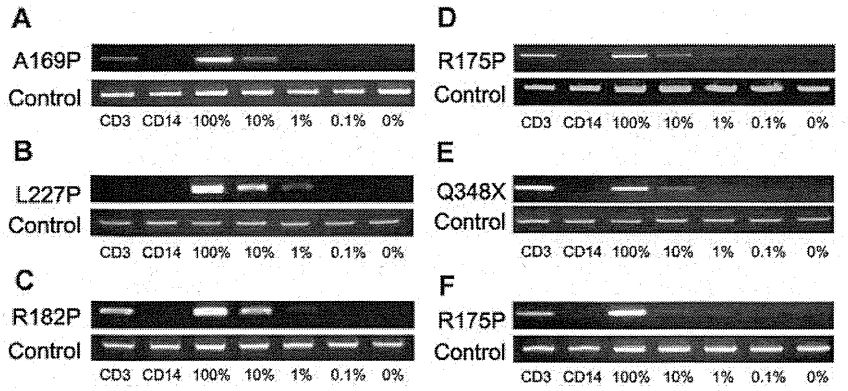

Figure 4. NEMO reversion selectively occurs in T cells of XL-EDA-ID patients. Allele-specific PCR for *NEMO* on $CD3^+$ or $CD14^+$ cells from (A) patient 4, (B) patient 5, (C) patient 6, (D) patient 7, (E) patient 8, and (F) patient 9. Numbers below each figure indicate the percentages of wild-type NEMO cDNA mixed with each mutant. Primers used in each PCR are shown on the left.

concordance between the degree of the disruption of *NEMO* gene and the proportion of reverted $NEMO^{normal}$ cells compared with $NEMO^{low}$ cells. The high proportion of reverted T cells seen in patients 1 and 2 as well as in patient 8 was associated with a highly disruptive mutation of the *NEMO* gene (ie, a duplication mutation in patients 1 and 2, and a truncation mutation in patient 8). In addition, the highly selective X-chromosome inactivation observed in the mothers of XL-EDA-ID patients indicated a strong selective advantage for $NEMO^{normal}$ cells over $NEMO^{low}$ cells. It is also noteworthy that reverted T cells were not detected in patient 5, who carried an L227P mutation that was not localized to either of the functional domains in the NEMO protein. Other reported cases with the same mutation presented with polysaccharide-specific humoral immunodeficiency and autoinflammatory diseases, but were spared complications such as cellular immunodeficiency and susceptibility to *Mycobacterium* (similar to patient 5).[4,8] This may reflect the fact that the L227P mutation in NEMO has less influence on T-cell growth than NEMO mutations that occur in functional domains, and suggests that reversion of the mutation has little impact on T-cell survival. Although the number of cases in our study is limited, it appears that the more disruptive NEMO mutations favor the survival of $NEMO^{normal}$ cells after reversion and X-chromosome inactivation.

Regarding the gradual decline in the number of NEMO-deficient T cells, one candidate trigger could be infection. Because the dominance of the memory phenotype and the skewed TCR repertoire among $CD8^+$ T cells in $NEMO^{normal}$ cells were observed in both patients 1 and 2 (Figure 1C and Mizukami et al[18]), continuous infection of pyogenic bacteria in patient 1 and *M szulgai* in patient 2 could be a reason for the emergence of $NEMO^{normal}$ cells and the elimination of $NEMO^{low}$ cells. The decrease in $NEMO^{normal}$ cells and restoration of $NEMO^{low}$ cells after anti-mycobacterial therapy in patient 2 support this hypothesis. In the case of patient 1, the predominance of $NEMO^{normal}$ T cells with an effector/memory phenotype at diagnosis (Table 4 and Mizukami et al[18]) is likely to be the result of chronic infection, and it is possible that $NEMO^{low}$ cells were predominant during his early infancy. Because some reports have indicated that TNF-α–induced programmed cell death of several cell types, including a human T-cell line, was enhanced by hypomorphic *NEMO* mutations,[12,35] and considering our finding that the levels of TNF-α expressed in revertant T cells were similar to levels in healthy control T cells in vitro (Figure 1F), TNF-α produced from these cells in response to infection could be involved in mutant T-cell elimination.

Unexpectedly, T-cell proliferation in patient 2 was equivalent to that of normal controls at the age of 2 months and was reduced after $NEMO^{normal}$ T cells increased (Figure 1B; Table 3). This finding indicates that the $NEMO^{low}$ T cells did not have intrinsically impaired mitogen-induced proliferation. One reasonable explanation for the reduced proliferation observed after the increase in $NEMO^{normal}$ T cells is a reduction in the absolute number of T cells (naive T cells in particular), probably because of the infection.

Table 5. Expression of mutant NEMO in various cell lineages for the mother of each XL-EDA-ID patient

Sample	Mutation	Analysis	Subtype	Mutant type, % (proportion)
Mother of patients 1 and 2	Duplication	FACS	CD3	0
			CD14	0
			CD19	0
Mother of patient 3	D311E	FACS	CD3	13
			$CD3^-$	54
		Subcloning	CD3	22 (6/27)
			$CD3^-$	55 (12/22)
Mother of patient 4	A169P	Subcloning	CD3	52 (11/21)
			CD14	58 (11/19)
			CD19	42 (5/12)
Mother of patient 8	Q348X	Subcloning	CD3	0 (0/26)
			CD14	17 (3/18)
			CD19	0 (0/18)
Mother of patient 10	1167insC	Subcloning	CD3	18 (7/39)
			CD14	12 (5/43)
			CD19	27 (12/44)

Data are shown as either the percentages of $NEMO^{normal}$ cells, as assessed by flow cytometry, or as the ratio of clones containing wild-type NEMO to the total number of clones, as analyzed by subcloning and sequencing analysis.